Composite Structures 331 (2024) 117916

Contents lists available at ScienceDirect

Composite Structures

journal homepage: www.elsevier.com/locate/compstruct

Impact response of composite energy absorbers based on foam-filled metallic and polymeric auxetic frames

Chuanqing Chen [a,b], Alessandro Airoldi [b,*], Antonio Maria Caporale [b], Giuseppe Sala [b], Xiaochun Yin [c]

[a] College of Engineering and Applied Sciences, Nanjing University, Nanjing, Jiangsu 210093, China
[b] Department of Aerospace Science and Technology, Politecnico di Milano, Milano, Italy
[c] Department of Mechanics and Engineering Science, School of Science, Nanjing University of Science and Technology, Nanjing 210094, China

ARTICLE INFO

Keywords:
Hexachiral auxetic
Foam-filled
Energy absorption
Localized impact

ABSTRACT

In this paper, an innovative concept is proposed, based on the hexachiral auxetic frames filled with foams with enhanced energy absorption capabilities. Numerical assessments of the composite foam-filled auxetic absorbers, of pure foam blocks and unfilled auxetic frames for metallic and polymeric material combinations were accomplished considering a case of localized impact. The energy absorbed by the composite absorbers are found superior to the sum of the energies absorbed by constituent elements tested separately with clear advantages also at the level of the specific energy absorbed per unit mass. The interactions between the two constituents are analyzed and discussed. An experiment considering a 3D-printed polymeric hexachiral frame filled with open-cell soft polyurethane foam under localized impact is conducted to validate the numerical approach. Eventually, a parametric sensitivity study is conducted numerically to illustrate the effects of geometrical parameters on the energy absorption capacity. Overall, the results confirm the potential and the great design flexibility of the concept, provides the guidelines to design advanced energy absorbing system, underlies the importance of the combination between the frame and foam properties and the effect of the main geometrical parameters on the performance.

1. Introduction

Auxetic material or structure, first named by Evans [1], are mechanical metamaterials with negative Poisson's ratio (NPR) behavior, which involves transverse shrinking under longitudinal compression and transverse expansion under longitudinal tension. As a consequence of their uncommon deformation pattern, auxetic materials and structures are endowed with many desirable material properties with respect to conventional ones, such as superior shear resistance [2,3], improved indentation resistance [2–9], enhanced fracture resistance [10–12], synclastic curvature behaviors [13,14], variable permeability [15,16] and better energy absorption capability [17–22]. By now, due to their superior physical–mechanical properties, auxetic metamaterials have been proposed as energy absorbers and protective barriers in several fields, such as in automotive [23,24], aerospace [25,26], sports equipment [27,28] and military [29] applications. Therefore, the study of enhancing, controlling, and tuning the indentation resistance, the impact response, and the energy absorbing abilities according to engineering demands is one of the most crucial objectives in the design of advanced absorbers based on auxetic structures.

Moving from the seminal work by Lakes [14], many types of auxetic materials have been proposed and studied, which can be classified according to the geometry and deformation mechanism into re-entrant, chiral, lozenge and square grid, rotating rectangle and triangle, and buckling-induced forms [30–33]. Chiral geometry is one of the most known class, due to its large auxetic effect. The hexachiral honeycomb concept was initially proposed by Prall and Lakes [34] and the in-plane Poisson's ratio of −1 was proven theoretically based on standard beam theory and confirmed experimentally. Subsequently, the tetrachiral, anti-tetrachiral, trichiral and anti-trichiral structures were proposed by Alderson et al. [35] and an hybrid chiral structure was described in [36]. Most of the 2D chiral mechanical metamaterials are based on periodic unit cell design, and their NPR is a characteristic of the topology, independent of the material, if the material is isotropic. Beside 2D chiral structures, some 3D chiral structures were also designed [37–43].

The impact resistance and the ability to absorb energy of auxetic

* Corresponding author.
E-mail address: alessandro.airoldi@polimi.it (A. Airoldi).

https://doi.org/10.1016/j.compstruct.2024.117916
Received 19 August 2023; Received in revised form 20 December 2023; Accepted 13 January 2024
Available online 14 January 2024

structures have been widely and recently studied [6,17,19–22,44–67]. For instance, Wang et al. [20] numerically investigated a novel crash-box made of an thin-walled tube filled with a re-entrant auxetic core under axial load. The results show that the energy absorption capacity of the crash-box by introducing an auxetic core improved without increasing excessively the peak impact force. Han et al. [44] numerically explored dynamic responses in 4-point star-shaped honeycomb structures. Using the energy absorption efficiency method and one-dimensional shockwave theory, they derived empirical formulas for densification strain and dynamic plateau stress to predict the dynamic load-bearing capacity of these honeycombs. Hu et al. [45] employed theoretical analysis to predict the dynamic NPR effect and crushing stress of the re-entrant hexagonal honeycomb, with validation through numerical results. The findings indicated an augmented NPR effect with an increase in cell-wall angle and a decrease in cell-wall length ratio. Additionally, honeycombs with small cell-wall angle, low relative density or high cell-wall length ratio exhibit heightened sensitivity to crushing stress at high impact velocities. Linforth et al. [47] evaluated the energy absorption capacity of an oval auxetic structure in dynamics and quasi-static experimental tests and developed a more favorable structure dubbed the 'Hybrid Auxetic Oval', which mitigated the effects of fracture. Gao and Liao [48] proposed a composite thin walled tube and proved an improvement of energy absorption performance by filling with double arrowed gradient auxetic structure. Gao et al. [49] numerically investigated the effects of relative density, topology parameter, initial impact velocity and mass on the in-plane impact performance of hex-chiral structures, which provides meaningful contributions to the optimization of chiral auxetic crashworthiness system. Zhang et al. [19] designed a bio-inspired re-entrant arc-shaped auxetic honeycomb structure. Compared with more conventional re-entrant hexagonal honeycombs, the new one performs a higher crushing load efficiency and a lower average stress fluctuation, which means a better energy dissipation capacity. Novak et al. [55] experimentally and numerically studied mechanical properties of the auxetic structures built from inverted tetrapods with a linearly graded porosity of under experimental impact test and observed an inclined non-constant plateau stress. Budarapu and Natarajan et al. [61] introduced a new conception of morphing airfoil with auxetic structures, which combined the advantages of larger deflections with limited straining of the components and auxetic deformation behaviors. It was numerically confirmed that the auxetic core has better mechanical performance than conventional ones.

It is worth noting that all these works proved that the auxetic structure have a superior energy absorption capacity with respect to other cellular configurations. However, the auxetic structures, like other cellular metamaterials, exhibit considerable porosity, which inevitably reduces their mechanical capability when subjected to load or impact. The achievement of some desirable properties, such as high shear resistance, indentation resistance, and energy absorption, is obtained in the auxetic structures with a topology where voids occupy a large part of the volume. Although, in most scenarios, the mechanical performance of auxetic metamaterials is still a better choice if compared with solid materials on a weight basis, some researchers explored the performance of composite absorbers by filling the voids in the frames with different lightweight materials.

The researches on these composite metamaterials are quite recent. Airoldi et al. [17] proposed an innovative concept for energy absorption, based on the combination of hexa-chiral auxetic structures and triangular foam prisms. The results show that the foam-filled hexa-chiral auxetic frame provides a superior energy absorption capability than that of the sum by the separate constituent elements. Ren et al. [68] studied the mechanical properties of the foam-filled auxetic circular tubes. They proved that the overall absorbed energy of combined structure is larger than the sum of single foams and hollow auxetic tube under compression. Novak et al. [69] designed uniform and graded hybrid metamaterial of 3D auxetic cellular structure filled by silicon and experimentally tested them under quasi-static and dynamic compression conditions. Results showed that the hybrid auxetic structure exhibits much better mechanical response with increased stiffness and smooth response than non-hybrid one. Zhou et al. [70] investigated the performance of the composite re-entrant auxetic structure filled by concrete foam with different densities subjected to quasi-static and low velocity compression. The experimental results showed that the energy absorption capacity of the structure increases with the density of the concrete foam filler. Yu et al. [71] studied the mechanical behaviors of a re-entrant hexagonal unit cell filled with foam, both experimentally and numerically. Compared to the hollow one, the foam-filled honeycomb obtained an improved specific energy absorption capability, resulting from a higher plateau stress. As the density of filling material increases, the structure could absorb more energy. Luo et al. [72] numerically and experimentally studied the mechanical properties and deformation patterns of slow recovery foam filled re-entrant honeycombs. The results show that energy absorption capacity of slow recovery foam filled re-entrant honeycombs increase with the increase of the strain rates, cell wall thickness and the decrease of cell angle. The ballistic impact tests of the foam-filled composite double-arrow auxetic structure were carried out by Liu et al. [73]. Compared to unfilled auxetic structure, both the energy absorption property and the ballistic limit velocity of foam-filled auxetic structures increased. Farrokhabadi et al. [74,75] assessed the energy absorption of auxetic structures infused with foam and reinforced with fiber-reinforced polymer matrix materials by both numerical and experimental methods. The findings reveal that the optimum specific energy absorption values are achieved when combining fiber reinforcement and foam filling.

As it can be seen from the above review, there is relatively limited research on the field of auxetic energy absorbers filled with foam and all the works have been focused on a specific type of foam and frame material combination. More systematic study on the properties of the two materials adopted for the frames and the filler, on their interaction, and on the mechanisms that leads to increase the energy absorption levels are missing. Moreover, there are no studies on the field of localized impact on foam-filled auxetic crash absorbers, with, at the best knowledge of the authors, one exception represented by the research presented in [17]. A localized impact event is actually more typical than uniformly crushing for structures as bumpers, helicopter subfloors, helmets and many other devices, but it is critical, since it is characterized by a small contact area and high stress, which produces plastic deformation and damages the structure even for low contact forces [76,77]. Actually, the auxetic behavior is particularly promising for localized impacts, since the NPR leads to densify the material under the impacted zone, but an effective exploitation of the auxetic response in such realistic conditions requires the transmission of the deformation from the locally impacted zone to the surrounding part of the absorber, which is critical if the materials undergo yielding or brittle failures that oppose or interrupt stress transmission. These issues, directly related to the non-linear response and to the failure limits of the frame, cannot be highlighted when an auxetic structure is uniformly crushed like in almost all of the studies presented in literature, because the auxetic effect is not required to be propagated from the impact zone to the surrounding material and it is not affected by frame failure. Accordingly, analyzing the mechanism of foam-filled auxetic structure deformation under localized impact is particularly important for real-world applications.

In this paper, a new hexachiral composite auxetic structure is proposed by filling foam into both the circular and triangular voids of an hexachiral auxetic frame, according to a concept illustrated in the second section of the paper. Then, the energy absorption performances of the new hexachiral composite auxetic structure in localized impacts are numerically studied in a third section for two combinations of materials based on metals and polymers, considering different types of foam-frame interactions, and highlighting the role of frame failures. Emphasis is given to absolute and specific energy absorption improvements with respect to both pure foam and unfilled frame absorbers. In

this first numerical study, the approach followed is similar to that validated in [17], and the new combination of materials, foam-frame interactions are mutually compared on a numerical basis, by using constitutive models calibrated with literature data. Then, an experimental activity conducted considering a polymeric 3D printed frame, filled by open-cell polyurethane foam is presented in the fourth section, together with the validation of the numerical approach for such choice of materials. Finally, the parametric sensitivity analysis of the new hexachiral composite auxetic structure is performed based on the validated numerical approach in the fifth section and the conclusions are summarized in the sixth section.

2. Concept and materials

2.1. Hexachiral cellular structure

Chiral cellular structures consist of circular elements acting as nodes, connected by ligaments tangent to the nodes. They can be classified into trichiral, tetrachiral or hexachiral structures, which have 3, 4 or 6 ligaments linked to one node, respectively. In this paper, the chiral hexagonal auxetic lattice structure is selected for the investigation of foam-filled auxetic absorbers. This kind of chiral auxetic structure exhibits negative Poisson's ratios of −1 under the rigid node assumption and full-wave shaped ligament deformation and exhibits good energy absorbing capabilities, if compared with other chiral topologies [35,78]. The chiral hexagonal auxetic structure consists of interconnected nodes and ligaments with six ligaments of the same length, L, which are tangentially linked to a node with outer radius r, as shown Fig. 1. The thicknesses of the ligaments and nodes are respectively denoted by t_n and t_l. The variables L, r, t_n and t_l represent the main geometrical parameters of the hexachiral auxetic network and L/r is a key parameter for the mechanical performance of the cellular structure [79].

2.2. Materials considered and related material models

In the activities presented in the first part of this paper, two types of composite hexachiral auxetic frames filled with foam were investigated numerically, by developing finite element models of localized impacts, solved through the Simulia/Abaqus Explicit code. The first one is a combination of metallic materials, consisting of a Titanium alloy frame filled with Aluminum foam (Al-foam) and the second one is a polymeric material combination consisting of Ultem 1000 frame filled with open-cell polyurethane CF-45M foam. Both Ultem 1000 and CF-45M foam are widely used in lightweight energy absorption applications [17,80]. The two types of combination will be referred to as metallic and polymeric composite absorbers, respectively. The material properties and the material models adopted in the Simulia/Abaqus simulations for these four types of materials are detailly introduced in the following.

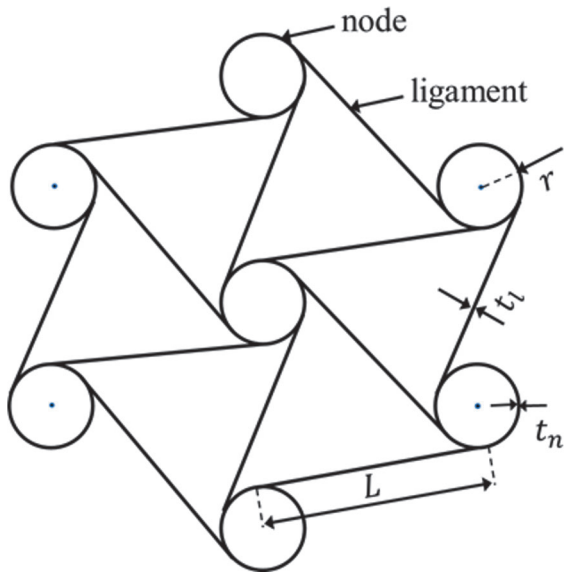

Fig. 1. Geometric parameters of hexachiral auxetic cell structures.

Owing to the excellent performance of specific strength and corrosion resistance, Titanium alloys are widely employed in aerospace and power engineering [80]. The most suitable method to produce a chiral frame in Titanium alloy is 3D printing, as shown in [78], where a Titanium Ti6Al4V alloy hexachiral unit was 3D printed by means of Selective Electron Beam Melting machine can be found in. In such work, the mechanical properties of the 3D printed material were measured by tensile testing of specimens, thus evaluating Young's modulus, yield stress, ultimate tensile strength, density and Poisson's ratio, which resulted equal to 102 GPa, 768.1 MPa, 854.55 MPa, 4430 kg/m^3 and 0.3, respectively. In the FE Abaqus models presented in this paper, Titanium alloy was modelled by using a classic Von Mises plasticity model and its failure strain was 0.0493 mm/mm as suggested in [78]. A ductile damage variable, which could represent the breakage of the ligaments or of the nodes beyond a plastic deformation threshold was also included in some analyses.

Aluminum foam is commonly used to withstand impact loading in real engineering applications, thanks to its superior stiffness-to-weight ratio, low density, good shear response, fracture strength, energy absorption and damping properties [81–83]. In this paper, an Al-foam was considered with a density of 230 kg/m^3, a Young's modulus of 0.11 GPa, a Poisson's ratio of 0.33 in elastic condition. During crushing the foam was characterized with a plateau stress of 1.75 MPa, on the basis of the data presented in Ref. [83]. In the Abaqus FE models, a constitutive law for crushable foam was utilized to simulate the behavior of materials that deform permanently during absorbing energy through crushing, such as metallic cellular foams. This law accounts for the typical asymmetric behavior in tensile and compressive responses by employing a flow potential surface with an elliptic projection in the meridian plane. Additionally, this law allows for the definition of a specific plastic Poisson's ratio, which was set to zero in the simulations presented and automatically defines a non-associated plastic flow. As illustrated in Refs. [80–83], this constitutive law permits the use of a maximum principal strain failure criterion to capture foam failure modes under uniaxial compression. To simulate the failure behavior of the Al-foam, a critical value of maximum principal strain was set at 0.4, beyond which elements were deleted. The value is identical to the failure strain value found in literature [85] investigating the compressive behaviors of closed-cell Al-foams.

For the frame of the composite polymeric metamaterial, unreinforced polyetherimide, commonly referred to as Ultem, was considered. Ultem is an advanced amorphous thermoplastic polymer with appealing thermal, electrical, and mechanical properties. The mechanical properties of Ultem 1000 have been widely investigated and can be found in the Ref. [86,87]. Following the data presented in such references, the Young's modulus, yield stress, ultimate tensile strength, density and Poisson's ratio are equal to 3280 MPa, 115 MPa, 167 MPa, 1280 kg/m^3 and 0.36, respectively. A classic Von Mises plasticity was adopted also in this case, but the material was characterized by a strain rate sensitivity, which was introduced by applying a dependency of the yield stress on the equivalent plastic strain rate, calibrated with the data presented in [86,87]. Such choice emphasized the role of the plastic response in the energy absorption performance of the ULTEM 1000 and was deemed adequate to represent the strain rate sensitivity of the polymeric ligaments, neglecting the viscous effects in the elastic range.

Analogously to the material model for the Titanium alloy, the breakage of polymeric ligaments was modelled by using a damage variable driven by plastic deformation (ductile damage). The failure strain was set as 0.02 mm/mm, which was evaluated through the numerical-experimental correlation in Section 4.

For the filler material in the composite polymeric metamaterial, the CF-45 M foam was considered, which is one of the commercially available versions of Confor® Open-celled urethane foams, currently applied in automotive and aerospace fields. Such open-cell foam has a density of 99 kg/m^3. Due to significant strain rate sensitivity of the response, three stress–strain curves at different strain rates were obtained from dynamic crushing and indentation tests by Airoldi et al. [17]. Such data were used to calibrate a material model specialized for low density foams with strain rate sensitivity (*Low Density Foam material [88]) in the following numerical simulations. The calibration was identical to the one presented in [17] and details are omitted for the sake of brevity. To simulate the failure behavior of CF-45M foam, a tension cutoff stress with elements deletion for low density foam was used. In the simulation presented such value was set to 1.4 MPa based on the numerical-experimental correlation later presented in Section 4.

Finally, it was assumed that strain rate sensitivity of the material has a significantly lower effect for metallic composite absorbers than for the polymeric ones. Accordingly, although the strain rate effects were considered for both the frame and the filler in the polymeric combinations, such aspect was neglected for the metallic elements in the numerical studies reported in section 3.

3. Evaluation of potential energy absorption performances of metallic and polymeric composite absorbers

In this paper, both polymeric and metallic materials were considered to investigate the concept of a composite energy absorber, obtained by completely filling both triangles and circular voids of an hexachiral frame with foam. In the numerical studies, two types of interaction were considered between the foam and the hexachiral frame: a simple contact and a glued condition. Since a tension cut-off was introduced at 1.4 MPa for the polymeric foam and a maximum principal strain at failure was included in the response of the aluminium foam, the foam material was subjected to tearing in the simulations, thus interrupting the connection with the frame, which results not infinitely strong. For such reasons, in the glued condition, the interaction was modelled with an ideal tied connection without failure, assuming that the adhesive that could be adopted to glue the foam with the frame was stronger than the foam. It was considered that such simplification would have not affected significantly the results obtained when considering a glued interaction. Moreover, this avoided the need for the introduction of contact or material models with failures to represent the adhesive, that should have been properly characterized when employed with a porous material such as the foam.

Additionally, the role of ligament breakage beyond certain level of plastic deformation was evaluated by comparing simulations including and excluding the activation of a damage variable within an elastic–plastic constitutive law. Such aspect is deemed to be particularly important for an understanding of the realistic performances of the absorbers.

To analyse quantitively the potential performances of the new foam-filled hexachiral frame in absorbing energy, the numerical models of dynamic localized impact for three types of absorbers including pure foam, pure auxetic frame and the composite foam-filled auxetic frame, were developed by using the Simulia/Abaqus Explicit solver and the results were compared and discussed. The numerical approach followed in this section is similar to the one validated in [17] and the performances of the different configurations are mutually compared on a numerical basis. An experimental validation of the approach for polymeric materials will be presented in section 4.

3.1. Numerical models

The finite element (FE) model of the pure foam specimens was modelled as a rectangular block of 192 mm × 420 mm, as shown in Fig. 2-a. A one-element wide slice, with a width of 1.0 mm, was represented and meshed with 3201 hexahedral elements having a reduced integration scheme (C3D8R elements) and 6642 nodes in the plane of the slice. The displacement along the Z-axis of the nodes of both sides of the block was constrained to avoid any displacement out of the plane of the modelled slice. The total masses of CF-45M foam and Al-foam were measured as 7.86 g and 18.10 g, respectively.

The FE model of a 192 mm long slice of the auxetic frame was developed, considering a width of 1.0 mm. The model is shown in Fig. 2 (b). The L/r parameter chosen for the evaluations presented in this section was 3.65. The ligaments and the circular nodes of the hexachiral frame had a thickness of 1.0 mm and were meshed by shell elements with a reduced integration scheme (S4R elements). A total number of 3282 elements and 6360 nodes were used. As in the FE model of pure foam, the displacement of Z-axis of the auxetic frame slice was

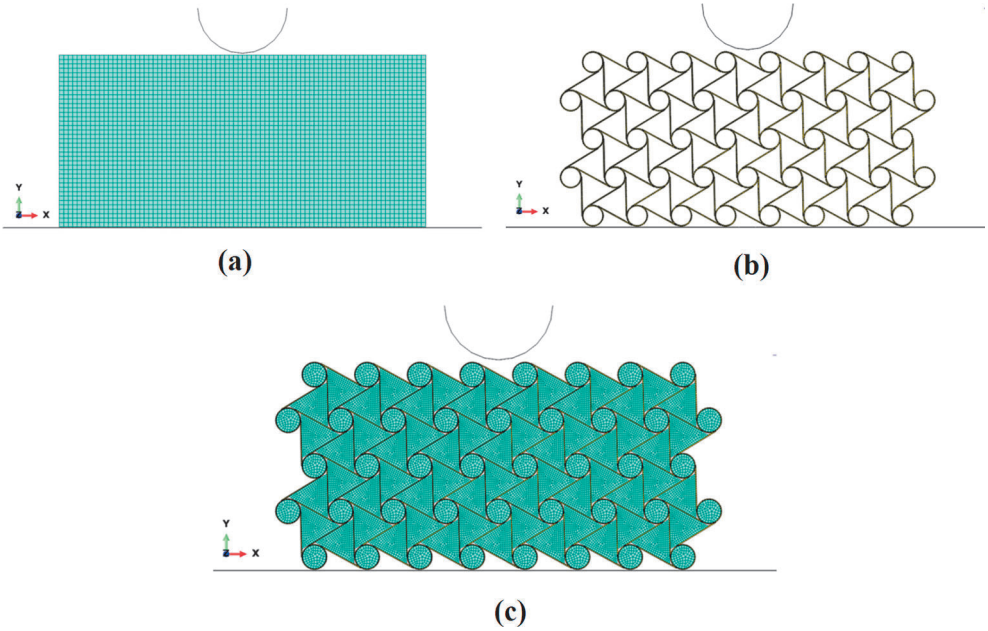

Fig. 2. FE models: (a) pure foam block, (b) pure auxetic frame, (c) foam-filled auxetic frame.

constrained to avoid any displacement out of the plane. The masses of Ultem 1000 frame and Titanium frame models were 9.46 g and 32.7 g, respectively.

To develop the numerical model of the foam-filled auxetic frame, the meshes of triangular foam prisms and the foam cylinders, made of hexahedral elements, were introduced into the voids of auxetic frame model previously described, as show in Fig. 2 (c). A total number of 19,404 elements and 43,500 nodes were used. The nodal displacement along Z-axis of both foam and auxetic frame elements were constrained to avoid any displacement out of the vertical plane. As anticipated, two interaction types between the filled foams and auxetic frame were used: a contact interaction (**General contact* with a friction coefficient of 0.2 [88]) and a glued condition, which was represented by using an algorithm available in Simulia/Abaqus to join dissimilar meshes (**Tie* algorithm [88]). The total masses of the polymeric and the metallic combination were 15.34 g and 46.28 g, respectively.

Throughout the work, a Matlab® script was used to generate all the FE meshes. The script is based on a parameterization of the hexachiral geometry and accomplishes initially the generation of the frame mesh. Then, two template meshes of the triangular and cylindrical foam inserts are scaled according to the prescribed dimensions and are subsequently rotated, translated, and copied in the correct positions to represent the foam fillers. The flowchart is sketched in Fig. 3.

For all the FE models, a localized impact was simulated. The impactor was modelled as a rigid cylindrical surface with radius of 50 mm. A rigid bottom plane was modelled below the specimens. A contact interaction was set between the impactor and the specimen as well as between the specimen and bottom plane (**General contact* with a friction coefficient of 0.2 [84]).

The potential energy absorption capabilities of the composite foam-filled frames with polymeric and metallic material combinations were evaluated through a total of 12 simulations, which are detailly listed in Table 1. The filled foam and frame were characterized by using the material models calibrated as explained in the previous sub-section.

The importance of the failure in the auxetic frame, beyond a certain value of plastic deformation, was investigated. Accordingly, the material of auxetic frame was simulated under two conditions: with failure behaviour (represented by "+" in Table 1) and without failure behaviour (represented by "-" in Table 1). The failure was represented by activating a ductile damage variable at a given onset deformation, which evolved quickly to completely degrade the material response, eventually leading to element deletion. The plastic deformation onsets (set be calibrating the **Initial damage* strain in Simulia/Abaqus [84]) were chosen by considering both literature and experimental data. In particular, for the Titanium alloy, the value of 0.0493 mm/mm was used as suggested in [78]. For the Ultem 1000 material, simulations with different values were performed in the initial phases of the activities, but the simulations presented in this section were performed by adopting a value of 0.02 mm/mm, which was evaluated through the numerical-experimental correlation that will be presented in Section 4.

Table 1
Material properties and initial conditions of FE simulations.

Case	Foam	Frame	Foam/frame Interaction type	Frame failure with ductile damage	Impact Velocity (m/s)
1	Al-foam	Titanium	Glued (G)	+	10
2	Al-foam	Titanium	Contact (C)	+	10
3	Al-foam	Titanium	Glued (G)	–	10
4	Al-foam	Titanium	Contact (C)	–	10
5	CF-45M	Ultem1000	Glued (G)	+	10
6	CF-45M	Ultem1000	Contact (C)	+	10
7	CF-45M	Ultem1000	Glued (G)	–	10
8	CF-45M	Ultem1000	Contact (C)	–	10
9	CF-45M	Ultem1000	Glued (G)	+	2
10	CF-45M	Ultem1000	Contact (C)	+	2
11	CF-45M	Ultem1000	Glued (G)	–	2
12	CF-45M	Ultem1000	Contact (C)	–	2

3.2. Performance indices

In the analysis of FE results, two quantitative indices were used to evaluate the energy absorbing capability, namely the total absorbed energy E and the Specific Energy Absorbed (SEA). The energy absorption is obtained by calculating the area integral of the force vs. displacement curve:

$$E = \int_0^{\delta} F d\delta \tag{1}$$

where F is the instantaneous impact force in the indentation direction, δ is the stroke distance, which represent the indentation for the localized impacts studied in this work.

The SEA index is given by:

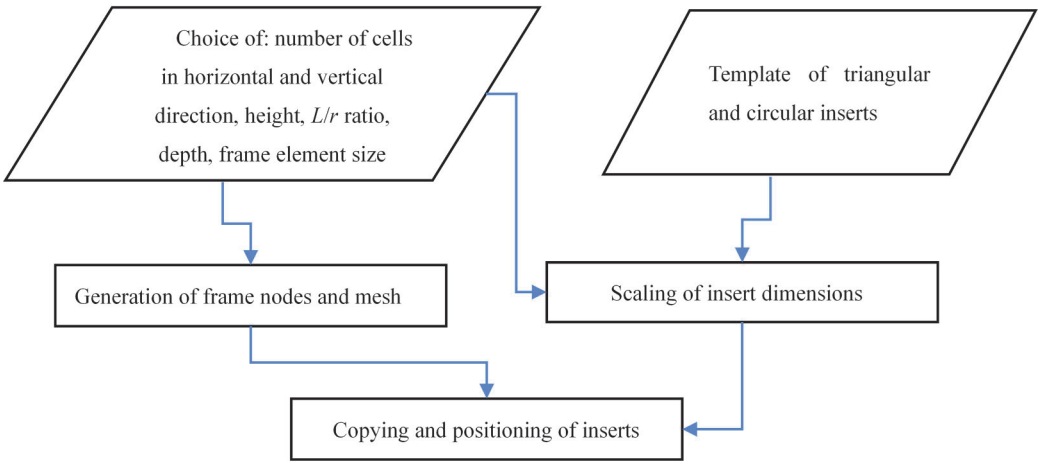

Fig. 3. Workflow of the automatic script for the generation of the foam-filled absorber mesh.

$$SEA = E/M_c \tag{2}$$

where M_c is typically the mass involved in the crushing of the absorber, so that $M_c = M_c(\delta)$. Actually, the simulation of a localized impact required a specific definition for the mass $M_c(\delta)$, which was defined as the mass of the absorbing material (foam and frame material) displaced by the impactor as it penetrates into the absorber, which was evaluated considering the volume of the impactor penetrated as a function of δ, as sketched in Fig. 4, and the average density of the different absorbers.

3.2.1. Performance of Titanium hexachiral frames filled by Al-foam

Four cases of Titanium auxetic frames filled by Al-foam under localized impact with initial velocity 10 m/s were simulated (cases 1–4 in Table 1).

An effective indentation displacement δ_f was defined to evaluate the performance indices, since after a given level of indentation, the connections between the parts of the absorbers at the side of the indenter are broken, and the energy absorption mechanism can change, even before the final densification. Accordingly, in this section of the paper, it was conventionally decided to evaluate the performance of the auxetic structure until the onset of damaging of the ligaments or nodes contained in the bottom layer of the structure. The fracture of the last layer of cell walls does not necessarily indicate bottoming initiation but results in a neat separation of the auxetic absorbers in two parts and a possible loose of the overall auxetic behaviour. By the observation of the collapse mode of Cases 1–4, it was found that an indentation $\delta_f = 100mm$ could be adopted to compare the performance of all the cases with metallic material combinations without including any effect of foam densification at the end of the indentation. The deformed configuration shown in the Fig. 4 is referred to the Case 2 for such indentation level.

The contact force vs. displacement curves of Cases 1–4 are shown in Fig. 5. The sum of the forces vs. displacement responses of the pure foam element and of the auxetic frame without foam filler is also reported in the plots presented Fig. 5. As it can be seen, for all cases, the forces of the foam-filled frame are generally slightly higher than the sum of pure foam and auxetic frame. The shaded region represents the difference between the areas under the forces vs. displacement responses of the foam-filled auxetic frame and of the auxetic frame without foam, so to intuitively demonstrate the contribution of filled foam to the performance of the composite frame.

It can be observed that the forces of the auxetic frames, both filled and unfilled, tend to increase with the indentation level. Such behaviour is not ideal, if the objective of the absorber is the maximum limitation of the force transmitted to the structure it protects for a given impact energy, but it is worth noting that this response to the localized impact could be optimized by functionally grading the properties of the absorbers. However, the ideal grading of properties is actually dependent on the indenter shape and impact conditions and is beyond the scope of the present work.

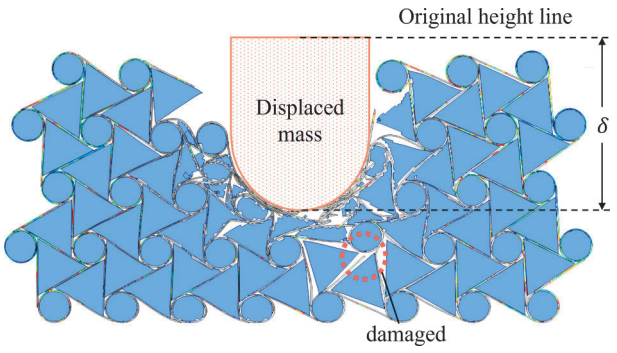

Fig. 4. Collapse mode of Case 2 and definition of displaced mass for SEA calculation.

In the Table 2, the energy absorption capabilities of all three types of absorbing elements at displacement 100 mm for Cases 1–4 are summarized. The increment of absorbed energy, ΔE, was calculated considering the performance of the foam-filled frame with respect to the sum of energies absorbed by the elements made of a single material. The increment of *SEA*, ΔSEA, obtained by the foam-filled frame is evaluated with respect both to the unfilled auxetic frame and to the pure foam block. As it can be seen from the Table 2, the composite absorber has a good improvement in the energy absorption capacity compared to the unfilled auxetic frame and to the pure foam block for all the cases. The highest increment of *E* is 26.82 %, while *SEA* increases both with respect to the auxetic frame (up to 14.9 %) and particularly with respect to the pure foam block (up to almost 100 %). Foam-Frame glued configurations (Cases 1, 3) performed better than the cases with simple contact interactions (Cases 2, 4), with an increment of energy between 5 % and 9 %. The introduction of ligament breakage in the simulations (Cases 1, 2) led to a significant drop of energy absorption capability with respect to the ideal case where ligaments were not allowed to fail: the model with damage absorb between 60 % and 65 % of the correspondent cases without damage. It is important noting that similar reductions occur both for the frame alone and for the composite absorber. The response of Case 1, with a realistic setting for ligament failure, is particularly interesting, considering that it was obtained without any optimization and sensitivity study: the SEA of aluminium foam was increased of almost 25 % thanks to effect of the auxetic frame.

3.2.2. Performance of Ultem 1000 hexachiral frames filled by CF-45M foam

Four cases of Ultem1000 auxetic frame filled by CF-45M foam under localized impact with an initial velocity 10 m/s were simulated, as mentioned in Table 1 (Cases 5–8). By the observation the collapse modes, the δ_f was set to 80 mm following the criterion of excluding the part of the response involving damages and failure in the bottom row of the frame nodes and ligaments. As in the case of the metallic composite metamaterial, this choice does not imply that bottoming initiated after δ_f, but rather indicates the near disappearance of correlation between the structures on either side of the indenter.

The force vs. displacement curves of Cases 5–8 are shown in Fig. 6. As it can be seen, the contact forces of the foam-filled frame are always significantly higher than sum of the contact force responses from the pure foam element and auxetic frame. However, in this case, the response of auxetic unfilled frame is characterized by a relatively constant force, while the response of the foam and of the filled auxetic frame tend to increase significantly with the indentation level.

The energy absorption capabilities of all three types of absorbing elements for Cases 5–8 are summarized in Table 3. It can be observed that the two quantitative indices of the pure foam are both better than those of unfilled auxetic frame, since the polymeric foam offers very high performances if compressed at high strain rates. The energy absorbed by the composite element is always higher than the sum of the energies absorbed by the single-material elements and there is a significant increment of ΔSEA of the foam-filled absorber with respect to the auxetic frame. The total energy of foam-filled frame has an increment between about 13 % and 50 % with respect to the sum of the two single-material absorbers and has at least a 97 % enhancement than the pure foam absorber for all four cases. However, the increments of *SEA* with respect to the foam are lower, and even negative for Case 6. These results can be summarized by stating that, considering a given volume available for absorber, the foam-filled auxetic frame can at least double the energy absorbing capabilities of the pure foam, and, in Cases 5, 7, and 8 this also occur with a neat *SEA* increment. As it can be seen from the Table 3, the foam-filled frame has always a considerable improvement in the energy absorption capacity with respect to the auxetic frame. The highest increasement of *E*, with respect to the sum of the energy absorbed by the two single-material absorbers, and *SEA*, with

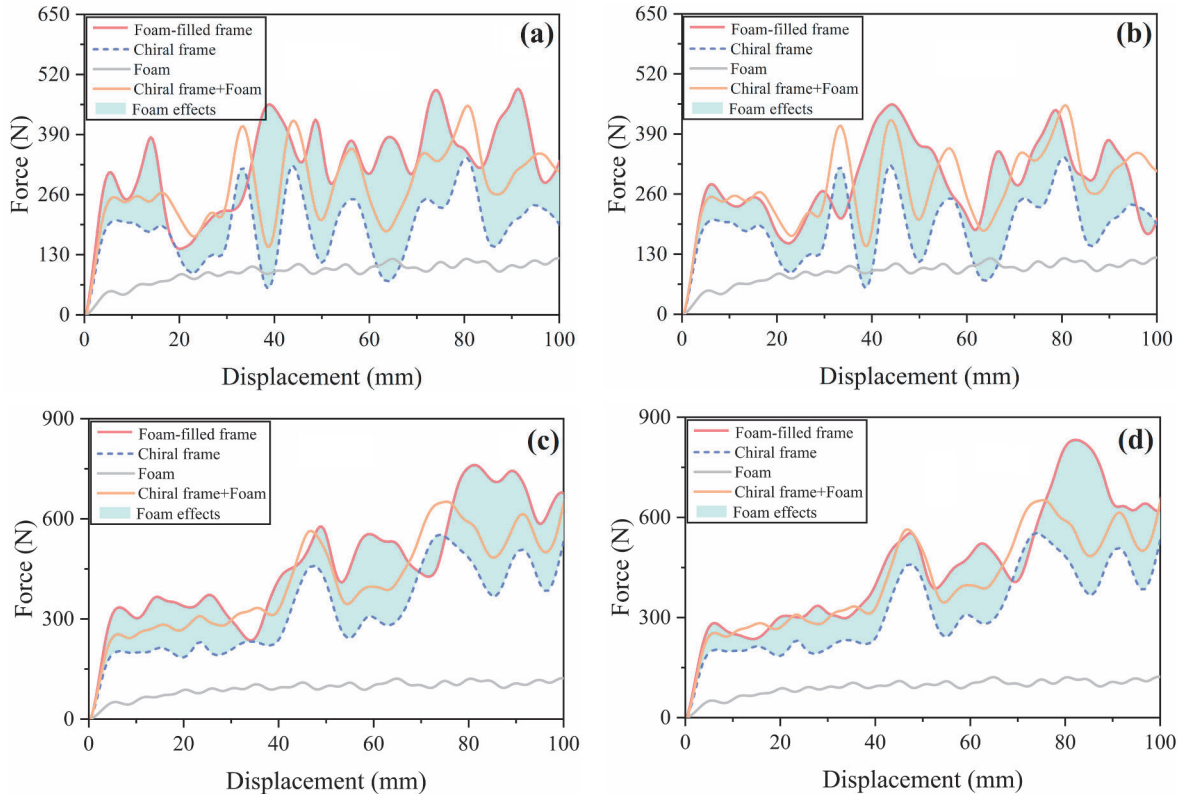

Fig. 5. Force vs. displacement of metallic absorbers: (a) Case 1, (b) Case 2, (c) Case 3, and (d) Case 4.

Table 2
Performances of metallic composite absorbers for a displacement of 100 mm.

Case	Foam block		Auxetic frame		Foam-filled frame		ΔE	ΔSEAframe	ΔSEAFoam
No.	E(J)	SEA(J/kg)	E(J)	SEA(J/kg)	E(J)	SEA(J/kg)	(%)	(%)	(%)
1 (G +)	8.30	4043	19.07	4381	31.11	5034	13.66	14.9	24.5
2 (C +)	8.30	4043	19.07	4381	29.61	4791	8.18	9.35	18.5
3 (G −)	8.30	4043	30.96	7114	49.79	8058	26.82	13.2	99.3
4 (C −)	8.30	4043	30.96	7114	45.47	7358	15.82	3.42	82.0

respect to the auxetic unfilled frame, are 47.28 % and 128.85 %, respectively. The influence of the type of foam-frame interaction is similar to those observed in the metallic combination. The introduction of the ligament failure leads to an energy absorption capability of 65 % for the unfilled frame with respect to the case without damage, while the energy absorption is less reduced for the composite absorber with a figure that is about 80 % of the case without damage. Accordingly, in this case, the composite absorber mitigated the detrimental effects of frame failures.

The importance of the polymeric foam strain rate sensitivity suggested to investigate the potential performances of the foam-filled hexachiral hybrid frame made of polymeric materials for a different impact velocity. Four cases of Ultem1000 auxetic frame filled by CF-45M foam under localized impact were analysed with initial velocity 2 m/s (Case 9–12 in Table 1). The observation of the collapse modes led to choose a limit $\delta_f = 80\,mm$ for the evaluation of performances.

The impact force vs. displacement curves of Cases 9–12 are shown in Fig. 7. As in Cases 5–8 with an impact velocity of 10 m/s, the impact forces of the composite auxetic frames resulted always much higher than the sum of the two absorbers made of a single type of material.

The energy absorption capabilities of all three types of absorbing elements for Cases 9–12 are summarized in Table 4. Since the energy absorption capability of the foam are lower for this lower impact velocity, the E and SEA of foam-filled frame are in this case always better than those of pure foam and pure frame. The combination of foam and frame materials appear well balanced and provide increments from 21 % to 86 % of total energy absorbed with respect to the sum of the two absorbers, and increment for about 4 % to 122 % of SEA with respect to the single-material absorbers. Accordingly, the foam-filled absorber provides considerable increments of energy absorption performances with respect to absorbers made of a single type of material if compared both on a weight and on a volume basis. The results of case 9, which includes ligament failure, can be remarked, since increments of 122 % with respect to the frame and of 52 % with respect to the foam block were obtained.

In a summary, for both metallic and polymeric materials, the quantitative indices indicated that the combination of the foam and the auxetic frame in the composite absorbers achieved significantly better performances than the absorbers made of a single material. It is worth noting that the geometrical parameters of the absorbers were not optimized to maximize energy absorption, so that these results can be considered very promising. The deformation mechanisms involved in the simulation of the foam-filled frame will be analysed in the following sub-section, highlighting the role of foam-frame interaction and of ligament failures.

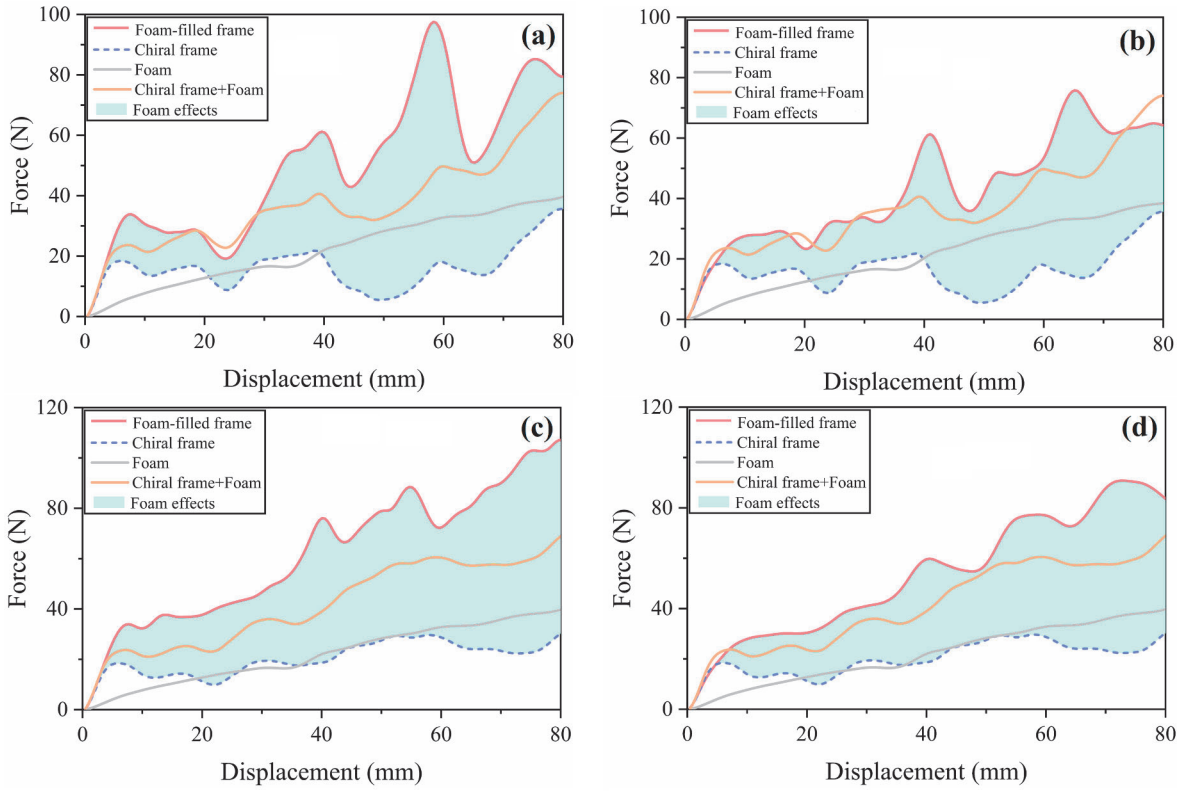

Fig. 6. Impact force vs. displacement of polymeric absorbers at 10 m/s impact velocity: (a) Case 5, (b) Case 6, (c) Case 7, and (d) Case 8.

Table 3
Performances of polymeric composite absorbers in 10 m/s impact velocity cases for a displacement of 80 mm.

Case	Foam block		Auxetic frame		Foam-filled frame		ΔE	ΔSEAframe	ΔSEAfoam
No.	E(J)	SEA(J/kg)	E(J)	SEA(J/kg)	E(J)	SEA(J/kg)	(%)	(%)	(%)
5 (G +)	1.79	2601	1.34	1140	4.15	2609	32.59	128.85	0.3
6 (C +)	1.79	2601	1.34	1140	3.53	2219	12.78	94.64	−14.6
7 (G −)	1.79	2601	1.70	1732	5.14	3232	47.28	86.60	24.3
8 (C −)	1.79	2601	1.70	1732	4.44	2776	27.22	60.27	6.7

3.3. Analysis of deformation mechanisms in the composite absorbers

The amplification effect on energy absorption of the foam-filled frame with respect to the absorbers made of single materials can be explained as a consequence of a double interaction between the auxetic frame and the deformable or crushable foam. A first phenomenon is the effect of the auxetic response of the frame on the foam material, which is attracted and densified under the impactor, thus allowing to extract more energy. A second effect is due to the densified foam, which sustains the ligaments of the frame during the deformation of the frame, delaying their buckling and providing alternative load paths in case of ligament failure.

In this sub-section, such interpretation will be assessed by analysing the role of the type of interaction modelled between the foam and the frame and the effect of the introduction of a ductile damage in the material model of the frame, which allows the representation of ligament breakage.

3.3.1. Effect of the interaction type between the foam and the frame

As presented in Table 1, some of the analyses were carried out by gluing the foam to the frame while others were performed by implementing a simple contact interaction between the foam and the frame materials. The different types of interaction affect the deformation of the structure under localized impact and have an effect on the energy absorption capacity. A comparison is presented in Table 5, where the E and SEA of all 12 cases are summarized directly comparing the cases with the contact and the cases with glued foam, all the other parameters being equal. Here, the ΔE and ΔSEA indices refer to the comparison between the cases that differ only for the different type of foam-frame interaction. The plus and minus signs indicate, as in Table 1, the simulation performed including (+) or excluding (-) the activation of the damage variable to represent the ligament breakage. The numerical results clearly indicate that the energy absorption capability of the absorber modelled with the foam glued to the frame is always better than the one of the corresponding cases with the foam just in contact with the frame. Since the masses of the two absorbers that are directly compared in each row are identical, the variation in the absolute and specific energy absorbed are identical as well.

In Fig. 8, the deformed structures of Case 5 and Case 6 during the impact process are reported. As it can be seen from Fig. 8 (a), referred to the simulation with the glued foam, the deformation of ligaments is apparently more restricted by the foam filler than in the case of Fig. 8 (b), referred to the case where the two materials are just in contact. The gap evidenced in Fig. 8 (a) is originated by the tension cut-off set to limit the tensile load carrying capability of the foam, which undergoes tension as it follows the ligament deformation (see Section 2.2). However, wherever the foam is able to carry the applied stress, it opposes effectively to the deformation of ligaments, as it can be seen by comparing

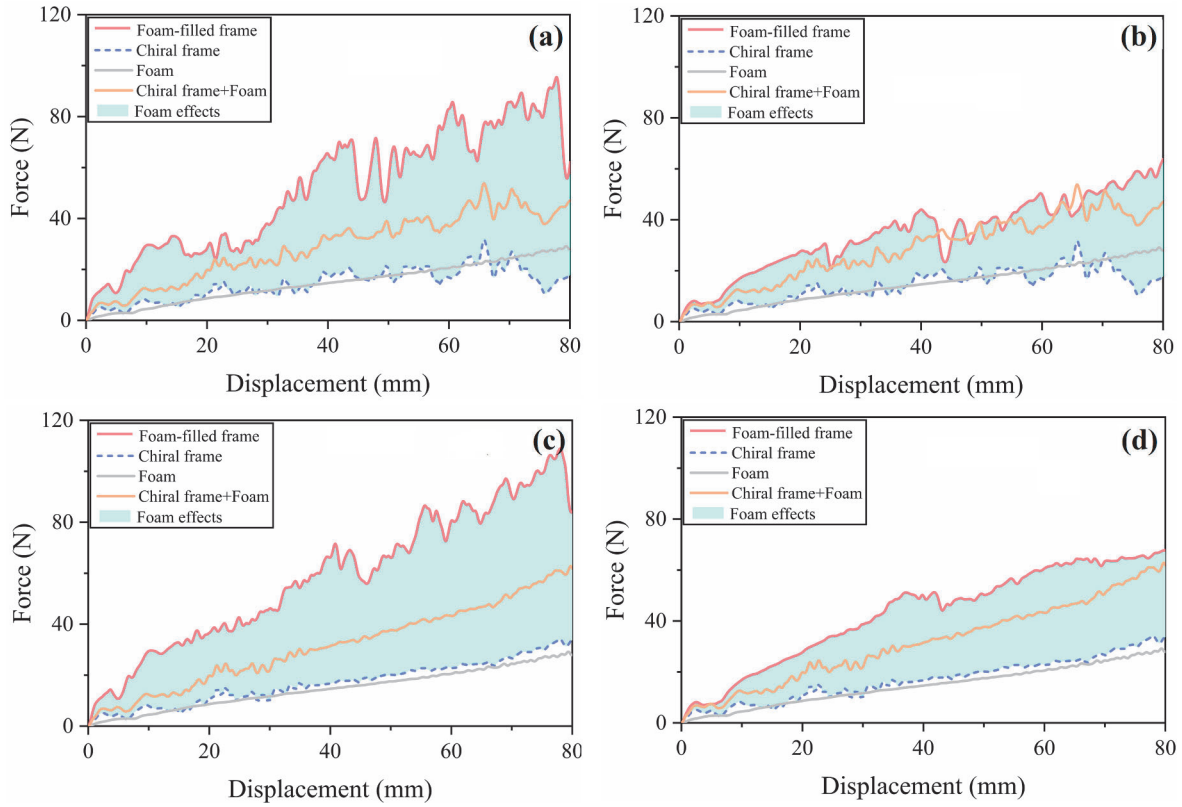

Fig. 7. Impact force vs. displacement of polymeric absorbers at 2 m/s impact velocity:: (a) Case 9, (b) Case 10, (c) Case 11, and (d) Case 12.

Table 4
Energy absorption performance of polymetric composite absorbers tested at 2 m/s impact velocity for a displacement of 80 mm.

Case	Foam		Auxetic frame		Foam-filled frame		ΔE	ΔSEAframe	ΔSEAfoam
No.	E(J)	SEA(J/kg)	E(J)	SEA(J/kg)	E(J)	SEA(J/kg)	(%)	(%)	(%)
9 (G +)	1.17	1695	1.14	1167	4.13	2593	78.79	122.19	52.1
10 (C +)	1.17	1695	1.14	1167	2.80	1759	21.21	50.72	3.78
11 (G−)	1.17	1695	1.36	1395	4.71	2962	86.17	112.32	74.8
12 (G−)	1.17	1695	1.36	1395	3.46	2174	36.76	55.84	28.3

Table 5
Comparison of energy absorption in the simulations of composite absorbers with different interaction types between foam and frame.

Cases "C" (with contact)	E(J)	SEA(J/kg)	Cases "G" (with glued foam)	E(J)	SEA(J/kg)	ΔE(%)= ΔSEA(%)
2 (+)	29.61	4791	1 (+)	31.11	5034	5.07
4 (−)	45.47	7358	3 (−)	49.79	8058	9.51
6 (+)	3.53	2219	5 (+)	4.15	2609	17.58
8 (−)	4.44	2776	7 (−)	5.14	3232	16.42
10 (+)	2.80	1759	9 (+)	4.13	2593	47.41
12 (−)	3.46	2174	11 (−)	4.71	2962	36.24

the configuration of the hexachiral frame under the impactor for the two cases. In the simulation with the simple contact implemented, the foam filler imposes less restriction to the bending of ligaments, as evidenced by the separations highlighted by circles in Fig. 8 (b) and this reduces the support provided against the buckling and the collapse of the ligaments and their breakage in the cases where the damage variable was activated (as in Cases 5 and 6). However, the quantitative comparison presented in Table 5 do not suggest a clear difference between cases where damage is activated and the other ones, so that the effects of the interaction and the ones of the ligament failure seem uncorrelated.

3.3.2. *Effect of the introduction of ligament breakage*

The purpose of this sub-section is to illustrate the effects of modelling the breakage of the frame on the energy absorption by comparing simulations where damage law was not activated with the ones where damage evolves after a plastic strain threshold and leads to element deletion when it reaches the unit value. The E and SEA of all 12 analyses cases are compared in Table 6 where, ΔE and ΔSEA refer to the performance of the cases without damage activation with respect to the cases with damage activation, all the other parameters being equal. The letter "G" and "C" indicate the cases with glued or simple contact interaction between foam and frame, respectively.

The drop of energy absorption capability consequent to the introduction of ligament breakage is considerable. All the cases without damage activated present a higher level of energy and specific energy absorbed (from 14 % to 60 % better).

The deformations of the composite auxetic structures were observed and analysed for achieving an insight on the phenomenon simulated. In Fig. 9, the displacement distributions along the horizontal axis in two simulations with polymeric material are compared for Case 5 (with damage activated) and Case 7 (without damage activated). The overall auxetic response of the absorbers is apparent from both the contours, since the left side moves toward the impactor (positive displacements along x-axis) as well as the right side (negative displacements along x-

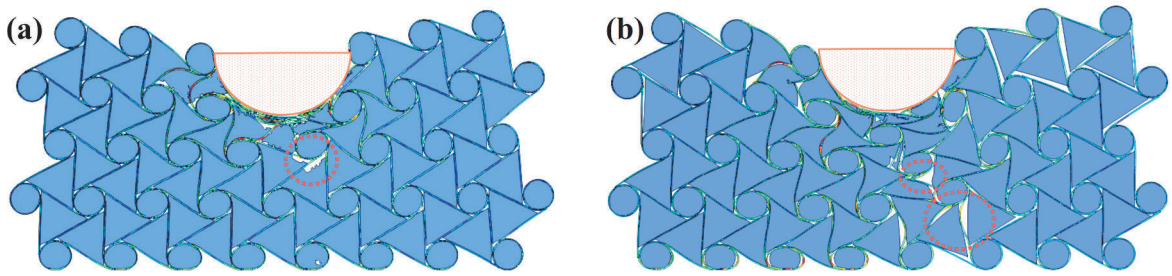

Fig. 8. Comparison of deformations of foam-filled auxetic structures with (a) foam glued to the frame (Case 5), (b) foam in simple contact with the frame (Case 6).

Table 6
Comparison of energy absorption in the simulations of composite absorbers with and without damage in frame materials.

Case + (with frame damage)	E(J)	SEA(J/kg)	Case - (without frame damage)	E(J)	SEA(J/kg)	ΔE(%) $=\Delta SEA$
1 (G)	31.11	5034	3 (G)	49.79	8058	60.07
2 (C)	29.61	4791	4 (C)	45.47	7358	53.57
5 (G)	4.15	2609	7 (G)	5.14	3232	23.88
6 (C)	3.53	2219	8 (C)	4.44	2776	25.10
9 (G)	4.13	2593	11 (G)	4.71	2962	14.23
10(C)	2.80	1759	12 (C)	3.46	2174	23.59

axis). Although the displacement distribution is different in the two cases, a clear quantitative difference cannot be noticed, considering the whole absorber. Some differences can be noticed at the local level, below the impactor. The activation of the damage variable produces a sudden transition between a zone where the frame pattern is slightly deformed and a zone where ligaments are broken into small fragments accumulated below the impactor, as shown in Fig. 9 (a). On the contrary, it is shown in Fig. 9 (b) that the deformation of the absorber in zone under the impactor is more progressive without the activation of damage variable. It is also worth noting, by comparing the force vs. displacement curves reported in Figs. 5, 6, and 7, that the simulations without the activation of damage are characterized by a lower amplitude of the force oscillations.

Considering that the activation of the damage induced a drop of energy capability also for the unfilled frame, as discussed in the previous Section 3.2, it can be stated that the breakage of the ligaments induced by damage affect directly the performance of the frame and have a local influence of the deformation of the foam under the impacted zone. The potential advantages offered by the adoption of a more ductile material for the frame are apparent form this analysis.

4. Experimental validation and sensitivity to geometrical parameters

The numerical activity presented in Section 3 indicated the potential of the foam-filled hexachiral absorber and highlighted the importance of some conditions. An experimental validation of the approach is hereby presented, considering a case that could be quite easily manufactured and with limited uncertainties related to the material characterization. For such a reason a polymeric combination of material and a simple contact interaction between foam and frame were considered, to partially validate the previous results and to increase the reliability of the following, additional sensitivity study on geometrical parameters. It is worth noting that the activities reported in [17] validated the model of the CF-45M foam, which was deemed acceptable for quantitative predictions.

4.1. Experiment test setup of localized impact

A localized impact experiment with an initial velocity 10 m/s between a hemispherical impactor and a 3D printed polymeric hexachiral auxetic frame filled by a visco-elastic foam was performed. The hexachiral auxetic frame consists of 4 cells in X-axis and 2 cells in Y-axis, and can be treated as a rectangular element, with a length of 418 mm, a height of 192 mm and a depth of 20 mm, as shown in Fig. 10. The thicknesses of the ligaments t_l nodes t_n were identical and set to 1.2 mm. The key parameter of the hexachiral structure L/r was set at 3.65. The hexachiral frame was meticulously crafted through Fusion Deposition Molding (FDM) using a Stratasys Fortus 450mc printer. A layer-by-layer printing approach was employed along its out-of-plane direction, as consistently depicted in the z-direction illustrated in Fig. 10 (a). In an effort to optimize printing quality while minimizing fabrication time, the layer thickness was finely tuned to 0.1 mm, and the printing speed meticulously adjusted to 30 mm/s, with a nozzle temperature set at 400 °C. Triangular prisms and cylinders were cut from a CF-45M foam block and inserted into the frame. The total mass of the foam-filled energy absorber resulted of 328.19 g.

The test was performed by using an impactor with a diameter of 100 mm and a mass of 12.1 kg, equipped with a hemispherical steel head. The set-up for the test is shown in Fig. 11 (a). In the test, the specimen was constrained between a set of aluminum guides to prevent lateral displacement during the collapse. The impactor was dropped from a height of 5 m, resulting in an initial impact velocity of 10 m/s for the experiment. The cylindrical body of the impactor was guided by a vertical hollow cylindrical tube. The deformation process was recorded by a high-speed camera. An acceleration sensor, connected to the acquisition

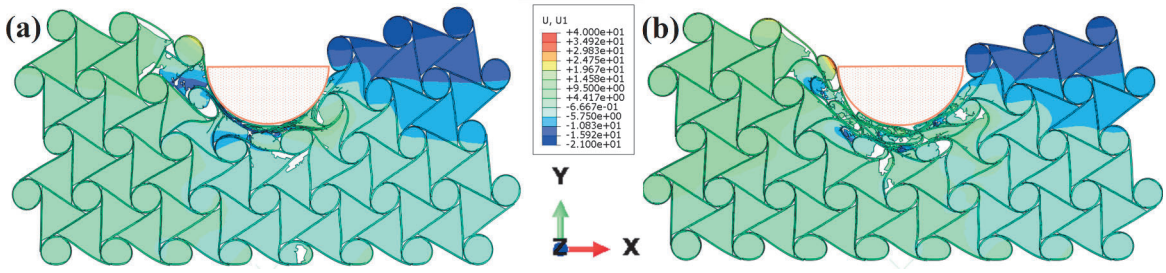

Fig. 9. Comparison of deformations of composite absorbers: (a) with the activation of damage variable (Case 5) and (b) without damage activation (Case 7).

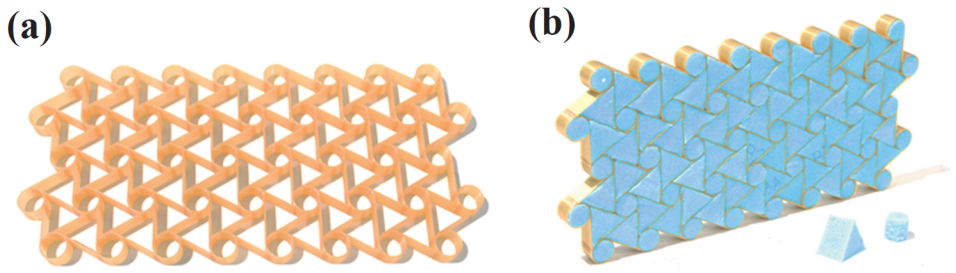

Fig. 10. Manufacturing of the polymeric composite absorber: (a) pure auxetic frame, (b) foam-filled auxetic frame.

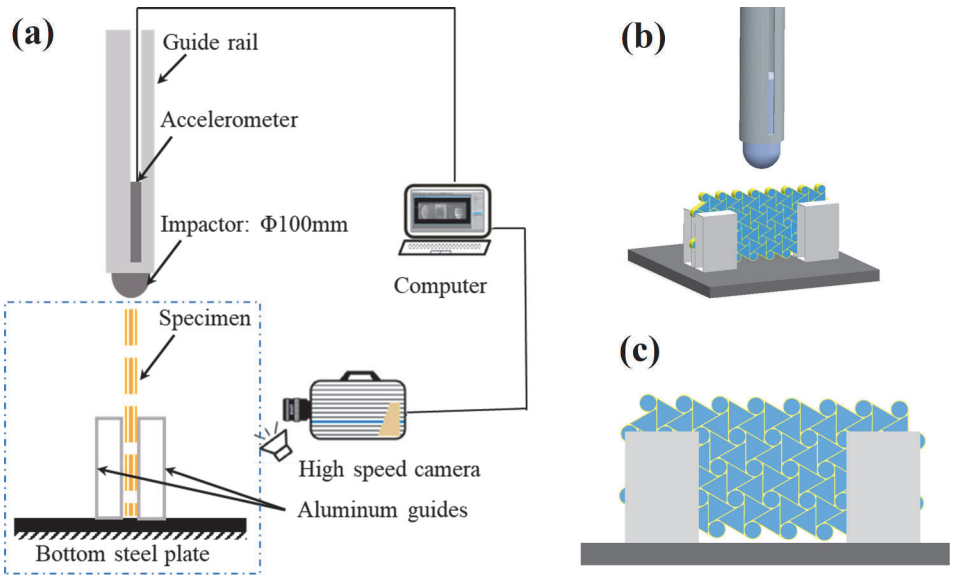

Fig. 11. (a) Set-up of the localized impact test, (b) 3D lay-out of the model of localized impact test, (c) front view of the 3D model of the specimen.

system through a data cable, was attached to the impactor to measure the acceleration, thus allowing to evaluate the impact force of impactor through Newton's second law.

4.2. Numerical approach

A FE model of the localized impact on the foam-filled auxetic structure was developed using the Simulia/Abaqus Explicit solver. Fig. 11 (b) shows the lay-out of the model of the localized impact test and Fig. 11 (c) shows the front view of model representing the items in the dashed box shown in Fig. 11 (a). The details of the model are presented in Fig. 12.

The model was generated through the script presented in Section 3.1. For the auxetic frame, the nodes and the linked ligaments were represented by shell elements (type *S4R* [88]) with a reduced integration scheme and a thickness of 1.2 mm. A contact interaction was introduced among all elements, with a friction coefficient of 0.2 (**General Contact* [88]). A total number of 164,200 solid hexahedral elements with a

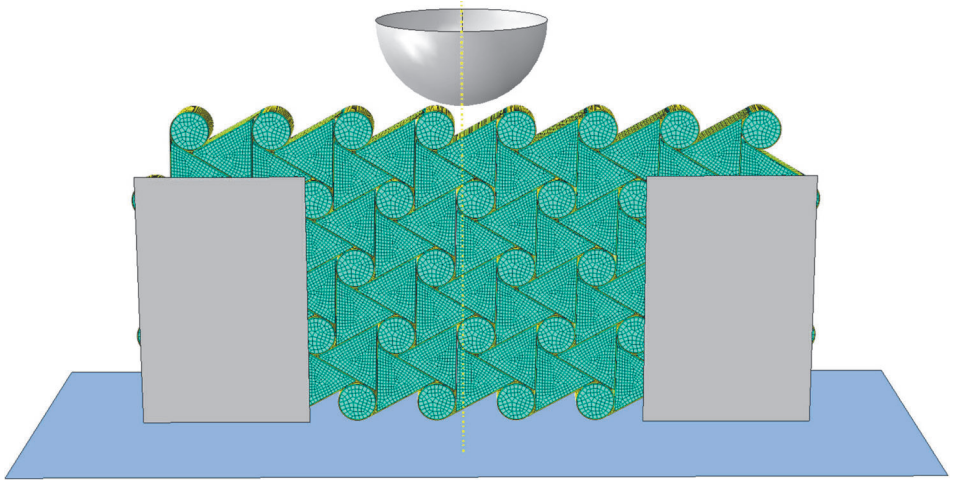

Fig. 12. FE model of the localized impact test.

reduced integration scheme (type *C3D8R* [88]) were used for the foam inserts. The impactor, the bottom ground surface and the vertical guides were represented by rigid elements, which were included in the general contact interaction defined for all the parts of the model. The bottom ground surface and the vertical guides were constrained in all directions. An initial vertical velocity of 10 m/s and a mass 12.1 kg were attributed to the reference node of the rigid body representing the impactor. Numerous studies have underscored the pivotal role of printing layer orientation and thickness as significant parameters that notably impact the physical properties of 3D-printed components [89]. Significantly, the perpendicular alignment of the printing direction with the loading direction mitigates material anisotropy introduced by FDM technology in the in-plane direction and minimizes the impact of interlayer bonding on the hexachiral framework's in-plane compression performance. Since the response of the frame mainly depend on in-plane properties, isotropy was considered a reasonable assumption for the property of ULTEM 1000 throughout the work. The auxetic frame and foam were characterized by using the material models of Ultem 1000 and CF-45 M foam, calibrated as in the previous sub-section 2.2. The only parameters that were varied during the model set-up to improve the correlation were the plastic deformation level for the onset of the damage in the polymeric frame, which was eventually set to 0.02 mm/mm, and the tension cutoff for the foam elements, finally set at 1.4 MPa. The total mass of the numerical foam-filled energy absorber resulted 335 g, which was almost equal to the specimen physically tested, with a small discrepancy of 2 %.

4.3. Numerical and experimental correlation

The collapse mode of the foam-filled hexachiral auxetic structure of both the numerical simulation and the experimental test are shown in Fig. 13. In particular, Fig. 13 (a), (b), (c), and (d) show four shots of structure's deformations at indenter displacements of 12 mm, 30 mm, 54 mm, 90 mm, respectively, while Fig. 13 (e), (f), (g) and (h) are the corresponding shots of numerical simulation. In the initial phase of the indentation, the collapse mode of the foam-filled absorber is characterized by the deformation of the nodes below the indenter, with a limited buckling of the connected ligaments. As the indentation proceeds, the dynamic failure mode is characterized by brittle failure of

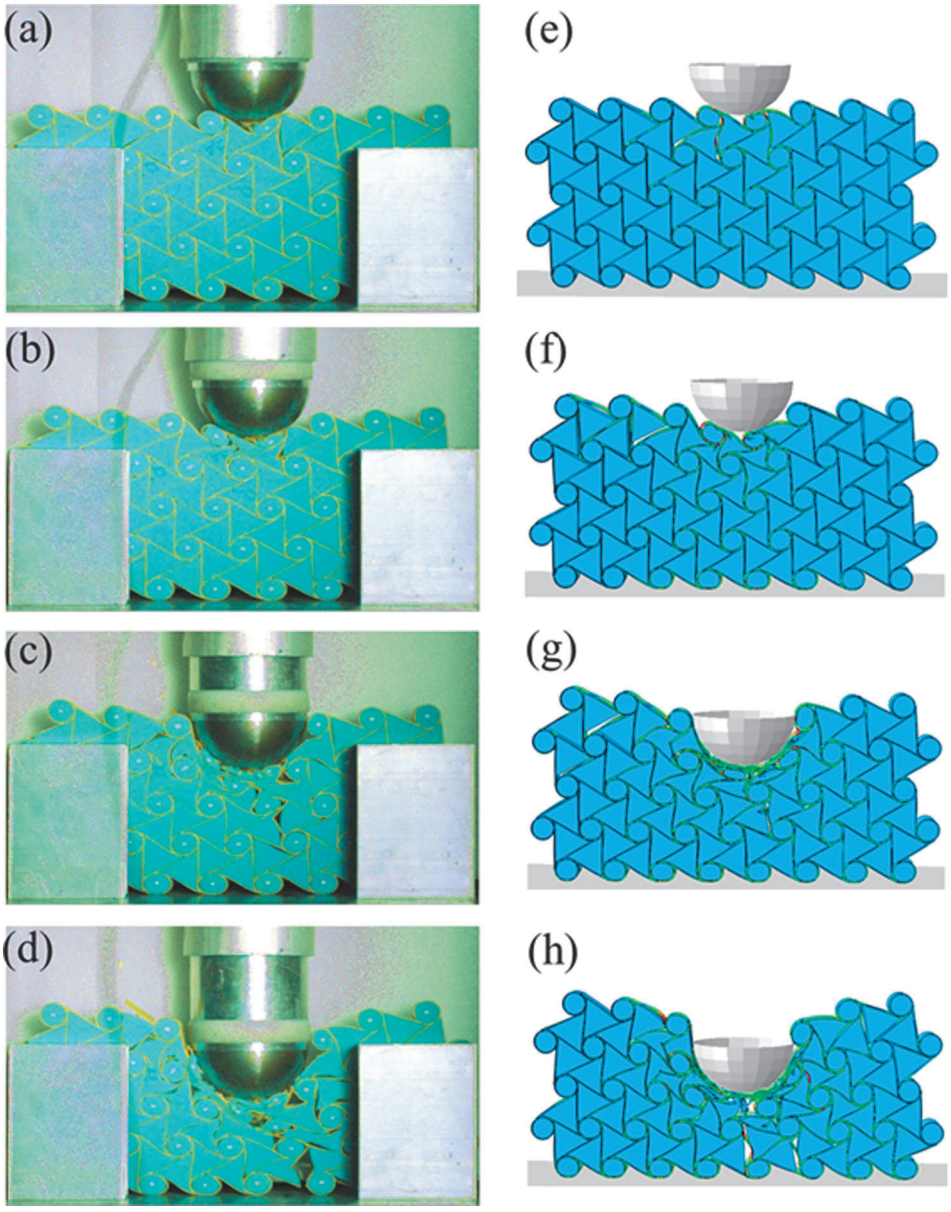

Fig. 13. Deformations of structure: experiment (a)-(d) and (e)-(h) FE model.

both ligaments and nodes. The foam inserts filled in the triangular and cylinders voids of the auxetic frame were progressively compressed below the indenter. There was an apparent development of gaps where the foam was not able to flow in the space created by ligament buckling and node collapsing. Such deformation mode was very well captured by the simulation. At about 90 mm of indentation, the ligament linked to the node at bottom of structure were damaged, thus leading to the failure of whole absorber. The simulation correctly represented the experimental response also in the final phase of the collapse.

The quantitative numerical-experimental correlation is presented in Fig. 14, where the force vs. displacement curve during the impact is reported. The experimental curve shows an initial ramp followed by a slightly increasing trend until about 90 mm. After 90 mm, the experimental curve presents a progressive load reduction, which started approximately in correspondence of the deformation shown in Fig. 13 (d) in the experiment. The curve progressively decreased, until a final bottoming occurring at about 180 mm.

The numerical results reported in Fig. 14 were filtered with a sae600Filter at a frequency of 600 Hz. Despite some differences in the high frequency oscillations, the trends of contact force–time curves of the experiment and of the FE model are substantially coincident. Overall, the results indicate that the modelling approach provided realistic predictions of the response of the foam-filled auxetic polymeric structure in dynamic localized impact.

4.4. Parameterized sensitivity analysis on the geometrical characteristic of the absorber

The assessment of the numerical model presented in Section 4.2 provided the basis for a sensitivity study focused on the role of geometrical parameters of the foam-filled absorbers consisting of Ultem 1000 frame and CF-45 M foam filler. The parameters considered were the cell wall thickness, t, and the ratio L/r. The cell walls of both ligaments and nodes were set to be identical, with three levels at 1.0 mm, 2.0 mm, and 2.5 mm. Four levels were considered for the L/r ratio, namely 3.65, 5.0, 7.0, and 8.0. The models were generated by using the Matlab ® script, mentioned in the Section 3.3.1.

Although the validation was conducted considering a specimen with a simple contact interaction between the frame and the foam, analyses were performed including also conditions with the glued foam. Impacts were simulated with the hemispherical 100 mm diameter rigid indenter adopted for the model of the validation experiment performed, at an impact velocity of 10 m/s. Considering the combination of L/r, wall thicknesses, and foam-frame interactions, a total number of 24 analyses were performed. The meshes and deformed configurations during the indentation of two analyses, referred to two different L/r ratio adopted, are presented in Fig. 15.

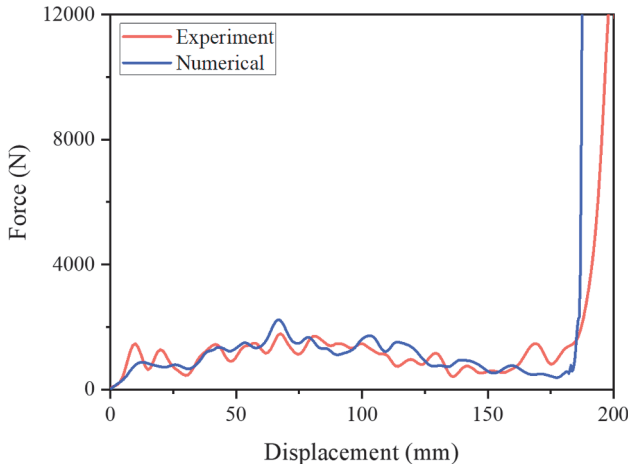

Fig. 14. Force vs displacement curves of experiment and numerical model.

The force vs. displacement and *SEA* vs. displacement curves obtained in the by using$L/r = 3.65$ and$L/r = 8.0$ are shown Fig. 16 and Fig. 17. The *SEA*-displacement curves were obtained by calculating the ratio of the energy absorbed during the process and the mass of the foam-filled material displaced by the indenter. As it can be seen, the impact force increases significantly as the cell wall thickness increases. The *SEA* vs. displacement curves present a peak at the beginning of the indentation and then the values stabilize at well-defined levels, which depend on all the design parameters considered in the study. The *SEA* values increase with the wall thickness and are, in general, higher for the glued foams with respect to the case of simple contact interaction. However, the beneficial effect of gluing the foam is really evident for the simulations with the thinnest thickness of cell walls, probably due to the more important role played by the foam filler. It can be also observed that the amplitude of the oscillations in the responses increases significantly with the thickness. The analysis of the other two cases with$L/r = 5.0$ and$L/r = 7.0$ confirms the previous observations.

The *SEA* results for the whole sensitivity study are summarized in the plots presented in Fig. 18, where the values are referred to given indentation δ_f, which were chosen by applying the same definition applied in section 2. However, the curves shown in Fig. 17 indicate that, after 75 mm of indentation, the *SEA* values do not undergo significant variations.

The results summarized in Fig. 18 confirm the role of the wall thickness of the frame in increasing the *SEA* results, which may easily exceed the performance of the pure CF-45 M foam absorber at 10 m/s for both the types of interactions. Values close to 4 kJ/kg can be reached if the thickness is increased at 2.5 mm, with an increment higher than 50 %. The role of the L/r ratio is more complex: results with $5 \leq L/r \leq 7$ are generally better than those at $L/r = 3.65$, but the cases with a wall thickness of 2 mm do not follow such a rule and exhibit a quite irregular trend. As already noticed in the analysis of Fig. 16 and Fig. 17, the glued condition presents evident superior performance only for a wall thickness of 1 mm, while its beneficial effect is clearly reduced and even canceled for higher thickness values.

5. Conclusions

In this paper, an innovative concept of a composite energy absorber was investigated considering a hexachiral frame filled with foams into its triangular and circular voids. The energy absorption performances were evaluated numerically in a localized impact condition. Both metallic and polymeric combinations of frame material and foam were considered by applying a numerical approach that was validated from the qualitative and quantitative point of view considering a test performed with polymeric materials. The performances in terms of absolute levels and specific values of energy absorbed per unit mass of the composite solutions resulted better than those of the corresponding constituent elements tested separately in the totality of the cases considered, with one single exception. Energy values absorbed by given volumes of materials and specific energy absorbed per unit mass can be doubled with respect to the levels achieved by unfilled frames or pure foam blocks.

The analysis of the results suggests that the auxetic response of the frame plays an important role in localized impacts, since it promotes the densification of the material under the indenter. For frames with relatively low thickness of the frame structures, it is also apparent that the densification of the foam delays the buckling of the ligaments, thus increasing the beneficial effects of the hybrid absorber.

The investigation of the role of ligament breakage is considered of particular importance for real-world applications. It was proved that such phenomenon must be taken into account if excessively optimistic predictions about absorption performances have to be avoided. However, the studies conducted, supported by an experimental validation,

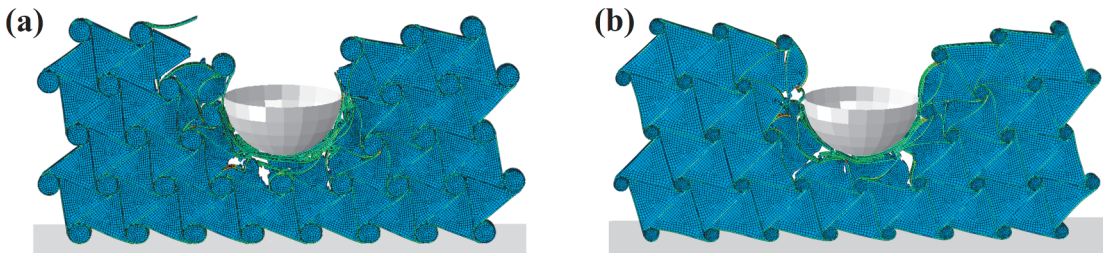

Fig. 15. Meshes and deformed configurations of polymeric composite absorber analyses with two different L/r ratios: (a) 5.0, (b) 7.0.

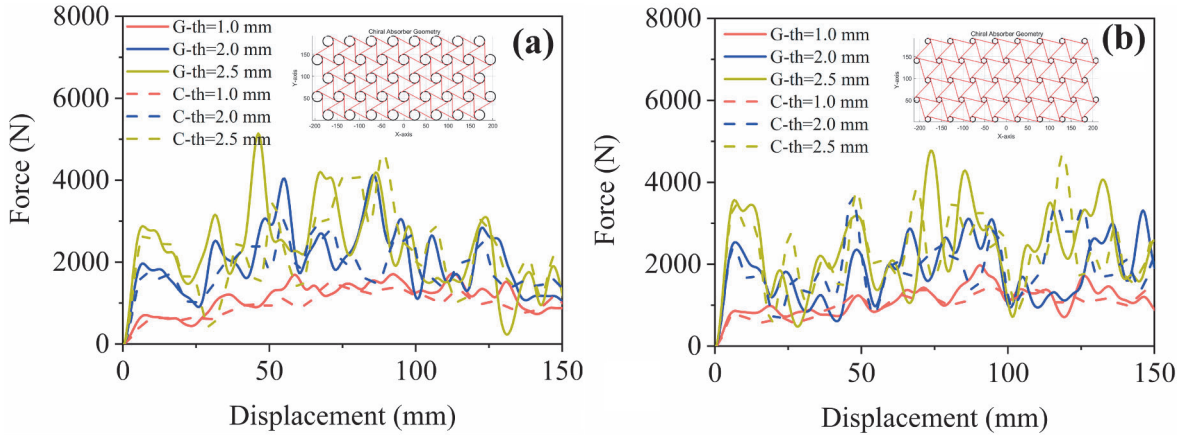

Fig. 16. Force vs displacement curves of impact simulations with polymeric composite absorber with different t: (a)L/r = 3.65, (b) L/r = 8.0.

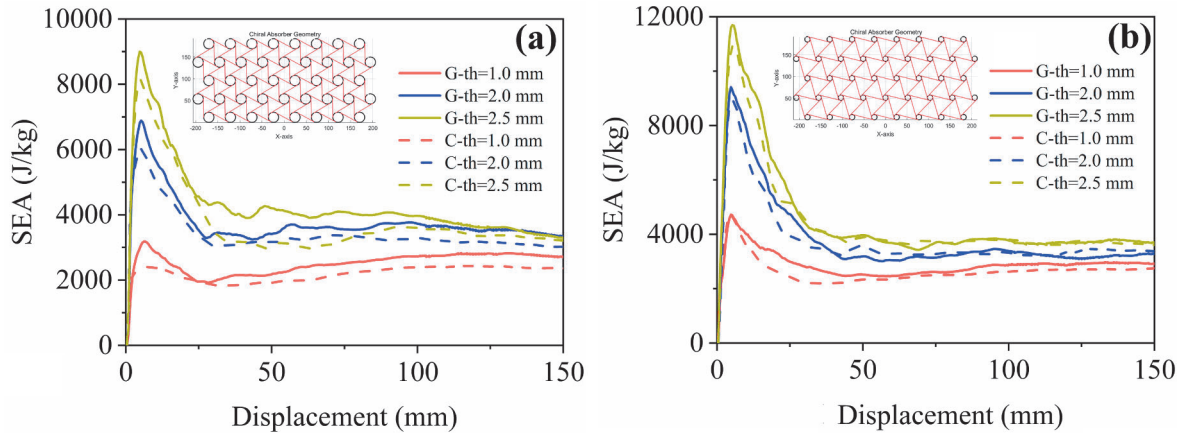

Fig. 17. *SEA* vs. displacement curves of impact simulations with polymeric composite absorber with different t: (a)L/r = 3.65, (b) L/r = 8.0.

indicate that the advantages presented by foam-filled auxetic absorbers are realistically achievable by real absorbers produced with feasible manufacturing techniques.

The design flexibility of the concept deserves additional considerations. It is apparent from these studies that an optimal combination between frame and foam material is a key factor to achieve the best performances. However, geometrical design parameters play also a very important role, so that optimal absorbers should be designed considering the specific requirements of the engineering applications, by means of numerical optimization methods. The development of parameterized models like the ones adopted in this work, which can be generated automatically, represents a first step in such a direction. Moreover, the possibility of varying the thickness of the frame and the type of foam for the insert should be emphasized, since it represents a feasible approach to develop functionally graded energy absorbers, capable of controlling the force levels during localized impacts and of providing different energy absorption performances for different levels of impact energy.

Therefore, the findings of this study are promising for the further development of the foam filled auxetic frames and useful to design enhanced energy absorber, especially in the case of localize impacts, in the fields of d aerospace, vehicle and civil engineering.

CRediT authorship contribution statement

Chuanqing Chen: Data curation, Investigation, Methodology, Software, Writing – original draft. **Alessandro Airoldi:** Conceptualization, Methodology, Project administration, Supervision, Writing – original draft, Writing – review & editing. **Antonio Maria Caporale:** Data curation, Investigation, Validation. **Giuseppe Sala:** Funding

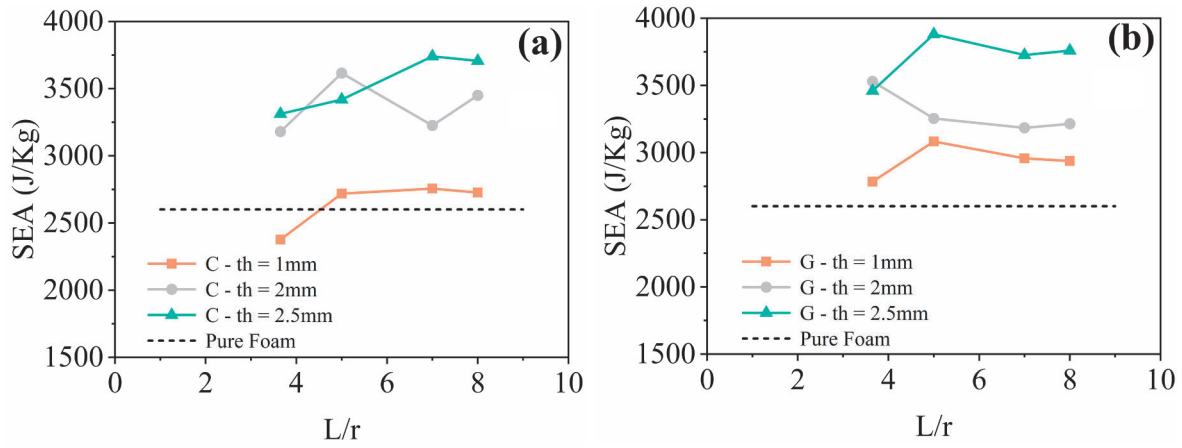

Fig. 18. *SEA* asymptotic values for analyses of localized impact on composite polymeric absorbers at 10 m/s: with simple contact interaction between foam and frame (a) and glued foam condition (b).

acquisition, Project administration, Resources, Supervision. **Xiaochun Yin:** Funding acquisition, Project administration, Resources, Supervision.

Declaration of competing interest

The authors declare that they have no known competing financial interests or personal relationships that could have appeared to influence the work reported in this paper.

Data availability

Data will be made available on request.

Acknowledgements

This study was carried out within the MOST - Sustainable Mobility National Research Center and received funding fron the European Union Next-Generation EU (Piano Nazionale di Ripresa e Resilienza (PNRR) - Missione 4. Componente 2, Investimento 1.4 - D.D. 1033 17/06/2022, CN00000023). This manuscript reflects only the authors' views and opinions, neither the European Union nor the European Commission can be considered responsible for them.

References

[1] Evans KE, Nkansah MA, Hutchinson IJ, Rogers SC. Molecular network design. Nature 1991;353:124. https://doi.org/10.1038/353124a0.
[2] Lakes R. Advances in negative Poisson's ratio materials. Adv Mater 1993;5:293–6. https://doi.org/10.1002/adma.19930050416.
[3] Francisco MB, Pereira JLJ, Oliver GA, Roque da Silva LR, Cunha SS, Gomes GF. A review on the energy absorption response and structural applications of auxetic structures. Mech Adv Mater Struct 2021:1–20. https://doi.org/10.1080/15376494.2021.1966143.
[4] Liu H, Chen L, Cao J, Chen L, Du B, Guo Y, et al. Axial compression deformability and energy absorption of hierarchical thermoplastic composite honeycomb graded structures. Compos Struct 2020;254:112851. https://doi.org/10.1016/j.compstruct.2020.112851.
[5] Zhu Y, Zeng Z, Wang Z-P, Poh LH, Shao Y. Hierarchical hexachiral auxetics for large elasto-plastic deformation. Mater Res Express 2019;6:085701. https://doi.org/10.1088/2053-1591/ab1a22.
[6] Hu LL, Zhou MZ, Deng H. Dynamic indentation of auxetic and non-auxetic honeycombs under large deformation. Compos Struct 2019;207:323–30. https://doi.org/10.1016/j.compstruct.2018.09.066.
[7] Chan N, Evans KE. Indentation resilience of conventional and auxetic foams. J Cell Plast 1998;34:231–60. https://doi.org/10.1177/0021955X9803400304.
[8] Alderson KL, Webber RS, Evans KE. Novel variations in the microstructure of auxetic ultra-high molecular weight polyethylene. Part 2: mechanical properties. Polym Eng Sci 2000;40:1906–14. https://doi.org/10.1002/pen.11322.
[9] Alderson KL, Fitzgerald A, Evans KE. The strain dependent indentation resilience of auxetic microporous polyethylene. J Mater Sci 2000;35:4039–47. https://doi.org/10.1023/A:1004830103411.
[10] Choi JB, Lakes RS. Fracture toughness of re-entrant foam materials with a negative Poisson's ratio: experiment and analysis. Int J Fract 1996;80:73–83. https://doi.org/10.1007/BF00036481.
[11] Alderson KL, Pickles AP, Neale PJ, Evans KE. Auxetic polyethylene: The effect of a negative poisson's ratio on hardness. Acta Metall Mater 1994;42:2261–6. https://doi.org/10.1016/0956-7151(94)90304-2.
[12] Liu Q. Literature Review: Materials with Negative Poisson's Ratios and Potential Applications to Aerospace and Defence; 2006.
[13] Chen YJ, Scarpa F, Liu YJ, Leng JS. Elasticity of anti-tetrachiral anisotropic lattices. Int J Solids Struct 2013;50:996–1004. https://doi.org/10.1016/j.ijsolstr.2012.12.004.
[14] Lakes R. Foam structures with a Negative Poisson's Ratio. Science 1987;235:1038–40. https://doi.org/10.1126/science.235.4792.1038.
[15] Jiang Y, Li Y. 3D printed auxetic mechanical metamaterial with chiral cells and re-entrant cores. Sci Rep 2018;8:2397. https://doi.org/10.1038/s41598-018-20795-2.
[16] Lim T-C, Acharya RU. Performance evaluation of auxetic molecular sieves with re-entrant structures. J Biomed Nanotechnol 2010;6:718–24. https://doi.org/10.1166/jbn.2010.1170.
[17] Airoldi A, Novak N, Sgobba F, Gilardelli A, Borovinšek M. Foam-filled energy absorbers with auxetic behaviour for localized impacts. Mater Sci Eng A 2020;788:139500. https://doi.org/10.1016/j.msea.2020.139500.
[18] Novak N, Starčevič L, Vesenjak M, Ren Z. Blast response study of the sandwich composite panels with 3D chiral auxetic core. Compos Struct 2019;210:167–78. https://doi.org/10.1016/j.compstruct.2018.11.050.
[19] Zhang X, An C, Shen Z, Wu H, Yang W, Bai J. Dynamic crushing responses of bio-inspired re-entrant auxetic honeycombs under in-plane impact loading. Mater Today Commun 2020;23:100918. https://doi.org/10.1016/j.mtcomm.2020.100918.
[20] Wang T, Li Z, Wang L, Hulbert GM. Crashworthiness analysis and collaborative optimization design for a novel crash-box with re-entrant auxetic core. Struct Multidisc Optim 2020;62:2167–79. https://doi.org/10.1007/s00158-020-02568-6.
[21] Simpson J, Kazancı Z. Crushing investigation of crash boxes filled with honeycomb and re-entrant (auxetic) lattices. Thin-Walled Struct 2020;150:106676. https://doi.org/10.1016/j.tws.2020.106676.
[22] Jiang H, Ren Y, Jin Q, Zhu G, Hu Y, Cheng F. Crashworthiness of novel concentric auxetic reentrant honeycomb with negative Poisson's ratio biologically inspired by coconut palm. Thin-Walled Struct 2020;154:106911. https://doi.org/10.1016/j.tws.2020.106911.
[23] Wang Y, Wang L, Ma Z, Wang T. Parametric analysis of a cylindrical negative Poisson's ratio structure. Smart Mater Struct 2016;25:035038. https://doi.org/10.1088/0964-1726/25/3/035038.
[24] Wang Y, Zhao W, Zhou G, Wang C, Gao Q. Parametric design strategy of a novel cylindrical negative Poisson's ratio jounce bumper for ideal uniaxial compression load-displacement curve. Sci China Technol Sci 2018;61:1611–20. https://doi.org/10.1007/s11431-017-9194-2.
[25] Airoldi A, Bettini P, Panichelli P, Sala G. Chiral topologies for composite morphing structures – Part II: Novel configurations and technological processes. Physica Status Solidi (b) 2015;252:1446–54. https://doi.org/10.1002/pssb.201584263.
[26] Airoldi A, Bettini P, Panichelli P, Oktem MF, Sala G. Chiral topologies for composite morphing structures – Part I: Development of a chiral rib for deformable airfoils. Physica Status Solidi (b) 2015;252:1435–45. https://doi.org/10.1002/pssb.201451689.
[27] Hernandez F, Shull PB, Camarillo DB. Evaluation of a laboratory model of human head impact biomechanics. J Biomech 2015;48:3469–77. https://doi.org/10.1016/j.jbiomech.2015.05.034.
[28] Allen T, Duncan O, Foster L, Senior T, Zampieri D, Edeh V, et al. Auxetic foam for snow-sport safety devices. In: Scher IS, Greenwald RM, Petrone N, editors. Snow

Sports Trauma and Safety. Cham: Springer International Publishing; 2017. p. 145–59. https://doi.org/10.1007/978-3-319-52755-0_12.
[29] Auxetic LSJ. Armour system for protection against soil blast loading. The University of Melbourne; 2020.
[30] Negrea RF. Brief review of metamaterials and auxetic materials. BUP-JAUTO 2021; 31:1–9. https://doi.org/10.26825/bup.ar.2021.003.
[31] Joseph A, Mahesh V, Harursampath D. On the application of additive manufacturing methods for auxetic structures: a review. Adv Manuf 2021;9: 342–68. https://doi.org/10.1007/s40436-021-00357-y.
[32] Kolken HMA, Zadpoor AA. Auxetic mechanical metamaterials. RSC Adv 2017;7: 5111–29. https://doi.org/10.1039/C6RA27333E.
[33] Ren X, Das R, Tran P, Ngo TD, Xie YM. Auxetic metamaterials and structures: a review. Smart Mater Struct 2018;27:023001. https://doi.org/10.1088/1361-665X/aaa61c.
[34] Prall D, Lakes RS. Properties of a chiral honeycomb with a poisson's ratio of — 1. Int J Mech Sci 1997;39:305–14. https://doi.org/10.1016/S0020-7403(96)00025-2.
[35] Alderson A, Alderson KL, Attard D, Evans KE, Gatt R, Grima JN, et al. Elastic constants of 3-, 4- and 6-connected chiral and anti-chiral honeycombs subject to uniaxial in-plane loading. Compos Sci Technol 2010;70:1042–8. https://doi.org/10.1016/j.compscitech.2009.07.009.
[36] Grima JN, Gatt R, Farrugia P-S. On the properties of auxetic meta-tetrachiral structures. Physica Status Solidi (b) 2008;245:511–20. https://doi.org/10.1002/pssb.200777704.
[37] Jiang Y, Li Y. Novel 3D-printed hybrid auxetic mechanical metamaterial with chirality-induced sequential cell opening mechanisms. Adv Eng Mater 2018;20: 1700744. https://doi.org/10.1002/adem.201700744.
[38] Fu M, Liu F, Hu L. A novel category of 3D chiral material with negative Poisson's ratio. Compos Sci Technol 2018;160:111–8. https://doi.org/10.1016/j.compscitech.2018.03.017.
[39] Duan S, Wen W, Fang D. A predictive micropolar continuum model for a novel three-dimensional chiral lattice with size effect and tension-twist coupling behavior. J Mech Phys Solids 2018;121:23–46. https://doi.org/10.1016/j.jmps.2018.07.016.
[40] Fu M, Zheng B, Li W. A novel chiral three-dimensional material with negative Poisson's ratio and the equivalent elastic parameters. Compos Struct 2017;176: 442–8. https://doi.org/10.1016/j.compstruct.2017.05.027.
[41] Frenzel T, Kadic M, Wegener M. Three-dimensional mechanical metamaterials with a twist. Science 2017;358:1072–4. https://doi.org/10.1126/science.aao4640.
[42] Ha CS, Plesha ME, Lakes RS. Chiral three-dimensional lattices with tunable Poisson's ratio. Smart Mater Struct 2016;25:054005. https://doi.org/10.1088/0964-1726/25/5/054005.
[43] Xia R, Song XK, Sun LJ, Wu WW, Li CL, Cheng TB, et al. Mechanical properties of 3D isotropic anti-tetrachiral metastructure. Phys Status Solidi B 2017.
[44] Han HL, Zhang XC. In-plane dynamic impact response characteristics of periodic 4-point star-shaped honeycomb structures. J Vibr Shock 2017;36:223–31.
[45] Hu LL, Zhou MZ, Deng H. Dynamic crushing response of auxetic honeycombs under large deformation: Theoretical analysis and numerical simulation. Thin-Walled Struct 2018;131:373–84. https://doi.org/10.1016/j.tws.2018.04.020.
[46] Najafi M, Ahmadi H, Liaghat G. Experimental investigation on energy absorption of auxetic structures. Mater Today: Proc 2021;34:350–5. https://doi.org/10.1016/j.matpr.2020.06.075.
[47] Linforth S, Ngo T, Tran P, Ruan D, Odish R. Investigation of the auxetic oval structure for energy absorption through quasi-static and dynamic experiments. Int J Impact Eng 2021;147:103741. https://doi.org/10.1016/j.ijimpeng.2020.103741.
[48] Gao Q, Liao W-H. Energy absorption of thin walled tube filled with gradient auxetic structures-theory and simulation. Int J Mech Sci 2021;201:106475. https://doi.org/10.1016/j.ijmecsci.2021.106475.
[49] Gao D, Wang S, Zhang M, Zhang C. Experimental and numerical investigation on in-plane impact behaviour of chiral auxetic structure. Compos Struct 2021;267: 113922. https://doi.org/10.1016/j.compstruct.2021.113922.
[50] Shepherd T, Winwood K, Venkatraman P, Alderson A, Allen T. Validation of a finite element modeling process for auxetic structures under impact. Physica Status Solidi (b) 2020;257:1900197. https://doi.org/10.1002/pssb.201900197.
[51] Gao Q, Zhao X, Wang C, Wang L, Ma Z. Crashworthiness analysis of a cylindrical auxetic structure under axial impact loading. Sci China Technol Sci 2020;63: 140–54. https://doi.org/10.1007/s11431-018-9467-6.
[52] Farokhi Nejad A, Alipour R, Shokri Rad M, Yazid Yahya M, Rahimian Koloor SS, Petrů M. Using finite element approach for crashworthiness assessment of a polymeric auxetic structure subjected to the axial loading. Polymers 2020;12:1312. https://doi.org/10.3390/polym12061312.
[53] Wang H, Lu Z, Yang Z, Li X. A novel re-entrant auxetic honeycomb with enhanced in-plane impact resistance. Compos Struct 2019;208:758–70. https://doi.org/10.1016/j.compstruct.2018.10.024.
[54] Tan HL, He ZC, Li KX, Li E, Cheng AG, Xu B. In-plane crashworthiness of re-entrant hierarchical honeycombs with negative Poisson's ratio. Compos Struct 2019;229: 111415. https://doi.org/10.1016/j.compstruct.2019.111415.
[55] Novak N, Borovinšek M, Vesenjak M, Wormser M, Körner C, Tanaka S, et al. Crushing behavior of graded auxetic structures built from inverted tetrapods under impact. Physica Status Solidi (b) 2019;256:1800040. https://doi.org/10.1002/pssb.201800040.
[56] Lee W, Jeong Y, Yoo J, Huh H, Park S-J, Park SH, et al. Effect of auxetic structures on crash behavior of cylindrical tube. Compos Struct 2019;208:836–46. https://doi.org/10.1016/j.compstruct.2018.10.068.
[57] Zhao X, Gao Q, Wang L, Yu Q, Ma ZD. Dynamic crushing of double-arrowed auxetic structure under impact loading. Mater Des 2018;160:527–37. https://doi.org/10.1016/j.matdes.2018.09.041.
[58] Gao Q, Zhao X, Wang C, Wang L, Ma Z. Multi-objective crashworthiness optimization for an auxetic cylindrical structure under axial impact loading. Mater Des 2018;143:120–30. https://doi.org/10.1016/j.matdes.2018.01.063.
[59] Foster L, Peketi P, Allen T, Senior T, Duncan O, Alderson A. Application of auxetic foam in sports helmets. Appl Sci 2018;8:354. https://doi.org/10.3390/app8030354.
[60] Qi C, Remennikov A, Pei L-Z, Yang S, Yu Z-H, Ngo TD. Impact and close-in blast response of auxetic honeycomb-cored sandwich panels: Experimental tests and numerical simulations. Compos Struct 2017;180:161–78. https://doi.org/10.1016/j.compstruct.2017.08.020.
[61] Budarapu PR, Y B SS, Natarajan R. Design concepts of an aircraft wing: composite and morphing airfoil with auxetic structures. Front Struct Civ Eng 2016;10: 394–408. https://doi.org/10.1007/s11709-016-0352-z.
[62] Shokri Rad M, Prawoto Y, Ahmad Z. Analytical solution and finite element approach to the 3D re-entrant structures of auxetic materials. Mech Mater 2014;74: 76–87. https://doi.org/10.1016/j.mechmat.2014.03.012.
[63] Scarpa F, Ciffo LG, Yates JR. Dynamic properties of high structural integrity auxetic open cell foam. Smart Mater Struct 2003;13:49. https://doi.org/10.1088/0964-1726/13/1/006.
[64] Rad MS, Hatami H, Alipouri R, Nejad AF, Omidinasab F. Determination of energy absorption in different cellular auxetic structures. Mech Ind 2019;20:302. https://doi.org/10.1051/meca/2019019.
[65] Teng XC, Ren X, Zhang Y, Jiang W, Pan Y, Zhang XG, et al. A simple 3D re-entrant auxetic metamaterial with enhanced energy absorption. Int J Mech Sci 2022;229: 107524. https://doi.org/10.1016/j.ijmecsci.2022.107524.
[66] Tan H, He Z, Li E, Cheng A, Chen T, Tan X, et al. Crashworthiness design and multi-objective optimization of a novel auxetic hierarchical honeycomb crash box. Struct Multidisc Optim 2021;64:2009–24. https://doi.org/10.1007/s00158-021-02961-9.
[67] Cheng X, Zhang Y, Ren X, Han D, Jiang W, Zhang XG, et al. Design and mechanical characteristics of auxetic metamaterial with tunable stiffness. Int J Mech Sci 2022; 223:107286. https://doi.org/10.1016/j.ijmecsci.2022.107286.
[68] Ren X, Zhang Y, Han CZ, Han D, Zhang XY, Zhang XG, et al. Mechanical properties of foam-filled auxetic circular tubes: Experimental and numerical study. Thin-Walled Struct 2022;170:108584. https://doi.org/10.1016/j.tws.2021.108584.
[69] Novak N, Krstulović-Opara L, Ren Z, Vesenjak M. Mechanical properties of hybrid metamaterial with auxetic chiral cellular structure and silicon filler. Compos Struct 2020;234:111718. https://doi.org/10.1016/j.compstruct.2019.111718.
[70] Zhou H, Jia K, Wang X, Xiong M-X, Wang Y. Experimental and numerical investigation of low velocity impact response of foam concrete filled auxetic honeycombs. Thin-Walled Struct 2020;154:106898. https://doi.org/10.1016/j.tws.2020.106898.
[71] Yu R, Luo W, Yuan H, Liu J, He W, Yu Z. Experimental and numerical research on foam filled re-entrant cellular structure with negative Poisson's ratio. Thin-Walled Struct 2020;153:106679. https://doi.org/10.1016/j.tws.2020.106679.
[72] Luo HC, Ren X, Zhang Y, Zhang XY, Zhang XG, Luo C, et al. Mechanical properties of foam-filled hexagonal and re-entrant honeycombs under uniaxial compression. Compos Struct 2022;280:114922. https://doi.org/10.1016/j.compstruct.2021.114922.
[73] Liu J, Yang W, Liu J, Liu J, Huang W. Ballistic impact analyses of foam-filled double-arrow auxetic structure. Thin-Walled Struct 2023;182:110173. https://doi.org/10.1016/j.tws.2022.110173.
[74] Farrokhabadi A, Veisi H, Gharehbaghi H, Montesano J, Behravesh AH, Hedayati SK. Investigation of the energy absorption capacity of foam-filled 3D-printed glass fiber reinforced thermoplastic auxetic honeycomb structures. Mech Adv Mater Struct 2023;30:758–69. https://doi.org/10.1080/15376494.2021.2023919.
[75] Farrokhabadi A, Mahdi Ashrafian M, Behravesh AH, Kaveh HS. Assessment of fiber-reinforcement and foam-filling in the directional energy absorption performance of a 3D printed accordion cellular structure. Compos Struct 2022;297: 115945. https://doi.org/10.1016/j.compstruct.2022.115945.
[76] Chen C, Yin X, Wang H, Jin T, Zhang L, Xie W, et al. Unloading behavior of low velocity impact between elastic and elastic–plastic bodies. Tribol Int 2020;151: 106485. https://doi.org/10.1016/j.triboint.2020.106485.
[77] Dong X, Yin X, Deng Q, Yu B, Wang H, Weng P, et al. Local contact behavior between elastic and elastic–plastic bodies. Int J Solids Struct 2018;150:22–39. https://doi.org/10.1016/j.ijsolstr.2018.05.020.
[78] Gunaydin K, Türkmen HS, Airoldi A, Grasso M, Sala G, Grande AM. Compression behavior of EBM printed auxetic chiral structures. Materials 2022;15:1520. https://doi.org/10.3390/ma15041520.
[79] Spadoni A, Ruzzene M. Numerical and experimental analysis of the static compliance of chiral truss-core airfoils. J Mech Mater Struct 2007;2:965–81. https://doi.org/10.2140/jomms.2007.2.965.
[80] Skripnyak VV, Skripnyak EG, Skripnyak VA. Fracture of titanium alloys at high strain rates and under stress triaxiality. Metals 2020;10:305. https://doi.org/10.3390/met10030305.
[81] Amaro AM, Neto MA, Cirne JS, Reis PNB. Mechanical characterization of different aluminium foams at high strain rates. Materials 2019;12:1428. https://doi.org/10.3390/ma12091428.
[82] Yao S, Chen Z, Xu P, Li Z, Zhao Z. Experimental and numerical study on the energy absorption of polyurethane foam-filled metal/composite hybrid structures. Metals 2021;11:118. https://doi.org/10.3390/met11010118.

[83] Zhao Y, Ma C, Xin D, Sun M. Dynamic mechanical properties of closed-cell aluminum foams with uniform and graded densities. J Mater Res 2020;35:2575–86. https://doi.org/10.1557/jmr.2020.157.
[84] Sun G, Wang E, Zhao T, Zheng G, Li Q. Inverse identification of cell-wall material properties of closed-cell aluminum foams based upon Vickers nano-indentation tests. Int J Mech Sci 2020;176:105524. https://doi.org/10.1016/j.ijmecsci.2020.105524.
[85] Li H, Zhang Y, Zhang J, Jiang C. Reconstruction and application of three-dimensional mesoscopic model of aluminum foam based on CT. J Beijing Univ Aeronautics Astronautics 2018;44:160.
[86] Mutter N. Characterization of dynamic and static behavior of polyetherimide. University of Central Florida; 2010. Master's Thesis.
[87] Zuanetti B. Characterization of Polyetherimide Under Static, Dynamic, and Multiple Impact Conditions. HIM 1990-2015 2013.
[88] Systèmes D. Abaqus Theory Guide (6.14). Simulia Corporation: Providence, RI, USA; 2014.
[89] Chuang KC, Grady JE, Draper RD, Shin E-SE, Patterson C, Santelle TD. Additive Manufacturing and Characterization of Ultem Polymers and Composites, Dallas, TX: 2015.